

Simulation-Based Classification; a Model-Order-Reduction Approach for Structural Health Monitoring.

T. Taddei · J. D. Penn · M. Yano · A.
T. Patera

Received: date / Accepted: date

Abstract We present a Model-Order-Reduction approach to Simulation-Based classification, with particular application to Structural Health Monitoring. The approach exploits (i) synthetic results obtained by repeated solution of a parametrized mathematical model for different values of the parameters, (ii) machine-learning algorithms to generate a classifier that monitors the damage state of the system, and (iii) a Reduced Basis method to reduce the computational burden associated with the model evaluations. Furthermore, we propose a mathematical formulation which integrates the partial differential equation model within the classification framework and clarifies the influence of model error on classification performance. We illustrate our approach and we demon-

This work was supported by OSD/AFOSR/MURI Grant FA9550-09-1-0613, ONR Grant N00014-11-1-0713, and the MIT-Singapore International Design Center.

Tommaso Taddei

Department of Mechanical Engineering, Massachusetts Institute of Technology, 77 Massachusetts Avenue, Cambridge, MA 02139 USA
E-mail: ttaddei@mit.edu

James D. Penn

Department of Mechanical Engineering, Massachusetts Institute of Technology, 77 Massachusetts Avenue, Cambridge, MA 02139 USA
E-mail: pennjam@mit.edu

Masayuki Yano

Institute for Aerospace Studies, University of Toronto, 4925 Dufferin St Toronto, ON M3H 5T6, Canada
E-mail: myano@utias.utoronto.ca

Anthony T. Patera

Department of Mechanical Engineering, Massachusetts Institute of Technology, 77 Massachusetts Avenue, Cambridge, MA 02139 USA
E-mail: patera@mit.edu

strate its effectiveness through the vehicle of a particular physical companion experiment, a harmonically excited microtruss.

Keywords Classification · model order reduction · parametrized partial differential equations · structural health monitoring

1 Introduction

In many engineering applications it is not possible to fully reconstruct the state of a physical system due to the deficiency of best-knowledge mathematical models and the limited quantity of experimental observations. However, it might still be possible to estimate Quantities of Interest (QOIs) on which we can rely to make engineering decisions. In this paper, we develop a computational approach which combines parametrized mathematical models and experimental data for the estimation of discrete-valued QOIs associated with physical systems.

From a mathematical standpoint, our goal is classification. We characterize our system by a finite number of exhaustive configuration classes. Then, we seek a function (*classifier*) g that maps experimental data to one of the anticipated configuration classes. We denote by $\mathbf{q}^{\text{exp}} \in \mathbb{R}^Q$ the raw data extracted experimentally, and we denote by $\mathbf{z}^{\text{exp}} \in \mathbb{R}^Q$ a set of functions (*features*) of \mathbf{q}^{exp} . Finally, we denote by $y \in \{1, \dots, K\}$ the (unknown) label associated with the configuration class of the current system. A classifier $g : \mathbb{R}^Q \rightarrow \{1, \dots, K\}$ should map the set of features \mathbf{z}^{exp} into the relevant configuration label y .

We shall focus on physical systems in which the crucial physical phenomena are described by Partial Differential Equations (PDEs). More precisely, we focus here on structural applications modelled by the elasticity equation. We shall denote by $\mu \in \mathbb{R}^P$ the set of parameters (material properties, geometric parameters) that collectively describe a system configuration. We shall further denote by $u^{\text{bk}}(\cdot; \mu)$ the best-knowledge approximation of the state of the system based on the PDE model for a given configuration μ (the \cdot anticipates an additional argument that will be introduced later). Finally, we shall denote by $\mathbf{z}^{\text{bk}}(\mu)$ the best-knowledge approximation of the experimental features.

Many engineering tasks, including monitoring, detection/identification, and (quality) control, can be recast as classification problems. There are a broad range of procedures that map data to class: some are described in terms of the application (e.g., Structural Health Monitoring, SHM, [26]), others are described in terms of the experimental approach (e.g., Acoustic Pulse Reflectometry, APR, [1,59]). In this paper, we shall focus on SHM although our approach is broadly applicable to a wide range of problems.

SHM refers to any automated monitoring procedure designed to assess the state of damage of a given aerospace, civil, or mechanical structure of interest. For civil engineering applications, SHM must provide real-time reliable assessment information regarding the integrity of a structure ([21]). In the aerospace industry, monitoring systems are required to assess the health of aircraft components during reconditioning or during the mission. In these contexts, SHM

is very similar in objective to Operational Loads Monitoring (OLM, [69,62]) and Integrated Vehicle Health Management (IVHM, [8,46]).

Several authors ([54,70]) have formalized the objective of SHM into levels of increasing difficulty. The first, and perhaps most important, level consists in assessing whether or not the structure is damaged. The second level consists in detecting the region of the structure in which damage is located and the type of damage. As observed independently by Farrar et al. in [25], and by Hurtado in [35], both these levels can be formulated as classification problems. In particular, the configuration label y introduced above is here associated with the *state of damage* of the structure.

In [25], a general paradigm for an SHM system is defined through the integration of four sequential procedures: operational evaluation, data acquisition, feature extraction, and statistical inference. *Operational evaluation* sets the limitations on what will be monitored and how the monitoring will be accomplished. During this stage, a formal definition of the potential states of damage is given. *Data acquisition* deals with the implementation of the sensing system. The sensing system can be based on static responses (in terms of strain ([56]) or displacement ([57,58])) or on dynamic (such as frequency) responses ([16,55]). Furthermore, sensing systems are referred to as *passive* if they rely on the ambient loading environment as an excitation source, and *active* if they can provide a local excitation tailored to the damage detection process (see, e.g., [26, Chapter 4.11]). *Feature extraction* identifies the vector-valued functions \mathbf{z}^{exp} of the acquired raw data \mathbf{q}^{exp} . Modal analysis ([67]) is the most widely-used feature-extraction technique; monitoring systems that rely on modal features are referred to as *vibration-based SHM* ([25, 24, 26]). Features based on modal properties are used for both passive and active sensing systems: Operational Modal Analysis (OMA, [2]) deals with the identification of modal properties of structures based on vibration data collected when the structure is in operation. Other popular techniques rely on Principal Component Analysis (PCA,[72]), or equivalently on Proper Orthogonal Decomposition (POD,[4,42]). Finally, the *inference step* deals with the development of a decision rule which serves to monitor the system.

There are two competing approaches to accomplish the inference step: the “inverse-problem” or “model-based” approach, and the “data-based” approach. Both approaches are based on an offline-online decomposition of the monitoring process: the *offline stage* is performed before the structure of interest starts to operate, while the *online stage* corresponds to the normal operations of the structure. In the *model-based approach* ([29]), a physics-based model (typically consisting of a set of differential equations) of the structure of interest is built and properly calibrated during the offline stage. During the online stage, this model is updated on the basis of the new measured data from the real structure. The solution to the updated model is then used to assess the state of damage of the system. Instead of proceeding from a law-based model, the *data-based approach* ([25,26]) is based on the collection of a dataset of offline training data from all the possible healthy and damaged states of interest. The dataset can be collected (i) by performing experiments on the structure

itself or on similar structures (see, e.g., [26]), or (ii) by performing synthetic experiments based on a (possibly parametrized) mathematical model of the structure of interest (see, e.g., [36,35,40]). Given the dataset, machine learning algorithms are used to train a classifier that assigns measured data from the monitoring phase to the relevant diagnostic class label. This classifier is then employed to monitor the structure during the online stage. The main limitation of the inverse-problem approach is that model updating is typically ill-conditioned, and confounded by many “nuisance” parameters, and hence not suitable for real-time computations. For this reason, most of the current research focuses on the data-based approach.

The main issue associated with the application of the data-based approach is the construction of the offline dataset used to train the classifier g . Since classification performances strongly depend on the amount of offline training data, the offline dataset should be representative of all possible system configurations (characterized by different geometries, and operational and environmental conditions) that can potentially occur online.

For practical applications, especially in civil SHM, it is extremely difficult to generate accurate offline datasets based on physical experiments: it is very rare that structures on the scale of bridges or dams become available for comprehensive testing. Furthermore, in most practical cases, data from the damaged condition of the structure are not available. For this reason, we may only consider outlier detection algorithms (see, e.g., [17]): we can assess whether or not the online measurements conform to the normal condition, reflected in the offline data, but we cannot ascertain the cause of any departure.

On the other hand, the use of simulations in the data-based framework presents two challenges. First, we need to estimate the solution to a parametrized PDE, $u^{\text{bk}}(\cdot; \mu)$ and then $\mathbf{z}^{\text{bk}}(\mu)$, for many values of the parameter $\mu \in \mathbb{R}^P$ (or, equivalently, for many system configurations). If we rely on a high-fidelity solver based on a Finite Element (FE) discretization the construction of the offline dataset leads to an unaffordable computational burden. For this reason, most of the early literature ([32,44]) resort to surrogate models, while more recent works focus on adaptive sampling schemes ([3,6,5,40]), in both cases to reduce the number of FE solves. Both these approaches face the problem of curse-of-dimensionality in the number of features Q and/or in the number of parameters P , and have been mostly applied to static data. Second, mathematical models are inevitably affected by model error. Errors in the model lead to errors in the construction of the dataset and consequently in the output of the learning algorithm. This source of error is extremely difficult to control, especially when we rely on surrogate models to generate the dataset.

As regards the first challenge, we propose a Simulation-Based Classification approach that relies on parametric Model Order Reduction (pMOR) to reduce the computational burden associated with the construction of the offline dataset without sacrificing the accuracy of the approximation. pMOR is a mathematical and computational field that aims to reduce the computational cost of the solution to a parametrized mathematical model in the limit of many queries. Among the different pMOR approaches proposed in the literature, in

this work we rely on the Reduced Basis (RB) method ([52, 50, 33]). We briefly summarize the distinguishing features of this methodology in section 4.3. While adaptive sampling techniques aim to reduce the number of datapoints required to train the classifier, our approach aims to reduce the computation cost for a given number of datapoints. For this reason, it is significantly less sensitive to the number of features Q . In future work, we propose a strategy based on component-based pMOR to address the curse-of-dimensionality in the number of parameters P .

As regards the second challenge, we further develop a rigorous mathematical formulation which couples the learning problem with the parametrized differential equation. Provided the availability of error bounds for the model error, this framework allows us to derive actionable estimates for the performance of the classifier based on synthetic data. Furthermore, it allows us to identify the distinct elements that combine to determine the performance of a monitoring system.

We can relate several features of our approach to existing methods. First, in [40], Lecerf, Allaire and Willcox already incorporate important aspects of model order reduction to accelerate the dataset construction within the data-based framework for aerospace applications. However, the reduction approach employed in [40] is based on a reduction of the dimension of the underlying PDE, and it does not exploit the parametric nature of the mathematical model. Furthermore, no error analysis is proposed to relate classification performances to non-parametric error in the mathematical model. Second, our error analysis takes advantage of tools first appeared in the robust optimization literature (see, e.g., [7, 10, 9]). In more detail, we rely on the ϵ -uncertainty indicator E^{bk} to measure the local robustness of a classifier g to data uncertainties; this quantity is equivalent to the stability radius first proposed in [34, 73].

The outline of the paper is as follows. In section 2, we introduce our framework through the vehicle of a particular example, a microtruss; in parallel we provide the abstraction applicable to a broad range of problems. In section 3, we describe the computational procedure, and we illustrate the role of pMOR. In section 4, we apply our approach to the microtruss problem: we present the classification results for both synthetic test data and real-data, and we demonstrate the importance of pMOR for the problem at hand. In section 5, we address questions related to the mathematical analysis of our formulation, and to the effect of model error. Finally, in section 6, we offer some concluding remarks and we anticipate a number of future developments.

2 A working problem: the microtruss example

In this section, we introduce the damage identification problem considered in this paper. We first introduce the experimental apparatus and procedure (section 2.1); then, following the general paradigm proposed in [25] and briefly outlined in the introduction, we provide an actionable definition of damage (section 2.2), we describe the data acquisition system, and we introduce the

experimental outputs (section 2.3). In section 2.4, we propose a parametrized mathematical model for the structure of interest which shall serve to estimate the experimental outputs, and we introduce a mathematical description of the space of system configurations. In section 2.5, we formalize the problem of feature extraction. Finally, in section 2.6, we state the classification problem and we summarize all the key definitions.

2.1 Experimental apparatus

We consider the acrylic microtruss system shown in Figure 1. The microtruss consists of a 4 by 4 grid of blocks of size $\ell_{\text{block}} \times \ell_{\text{block}}$, $\ell_{\text{block}} = 0.25[\text{in}]$, linked together by horizontal and vertical joints of size $L_{\text{joint}} \times h_{\text{joint}}$, $L_{\text{joint}} = 1[\text{in}]$ and $h_{\text{joint}} = 0.015[\text{in}]$. The depth of the microtruss is equal to $d_{\text{mtruss}} = 1[\text{in}]$. We state upfront that the actual geometry of the microtruss is to be considered uncertain due to the (3d-printing) manufacturing process. For this reason, the values reported above should be interpreted as nominal, and we shall refer to the configuration described above as the *nominal geometry*. We resort to cartesian coordinates; since the geometry is independent of the third dimension, we use notation

$$x^{\text{dim}} = L_{\text{joint}} x = L_{\text{joint}} x_1 \mathbf{e}_1 + L_{\text{joint}} x_2 \mathbf{e}_2 = L_{\text{joint}} \begin{bmatrix} x_1 \\ x_2 \end{bmatrix}$$

to indicate a physical point in the microtruss; here \mathbf{e}_1 and \mathbf{e}_2 are the canonical unit vectors, and $L_{\text{joint}} = 1[\text{in}]$ is the non-dimensionalization constant. In what follows we exclusively refer to non-dimensional quantities unless otherwise indicated. We refer to the blocks using the matrix notation (i, j) , $i, j = 1, \dots, 4$: the i -index corresponds to the x_1 position and is ordered from left to right in Figure 1(b); the j -index corresponds to the x_2 position and is ordered from bottom to top in Figure 1(b).

Our goal is to detect the presence of added mass on top of block (1, 4) and of block (4, 4). More precisely, we wish to distinguish between $K = 4$ states of damage: no added mass ($y = 1$), added mass on top of block (1, 4) ($y = 2$), added mass on top of block (4, 4) ($y = 3$), added mass on top of both block (1, 4) and block (4, 4) ($y = 4$). We refer to the case of no added mass as the undamaged case. Figure 1(c) shows the detail of the added mass on top of block (1, 4) for a particular experimental configuration. Added mass is of the same material as the microtruss system.

2.2 Definition of damage

In view of the definition of damage, we first introduce the non-dimensional ratios

$$s_L := 1 + \frac{V_{\text{left}}}{V_{\text{nom}}}, \quad s_R := 1 + \frac{V_{\text{right}}}{V_{\text{nom}}}, \quad (1)$$

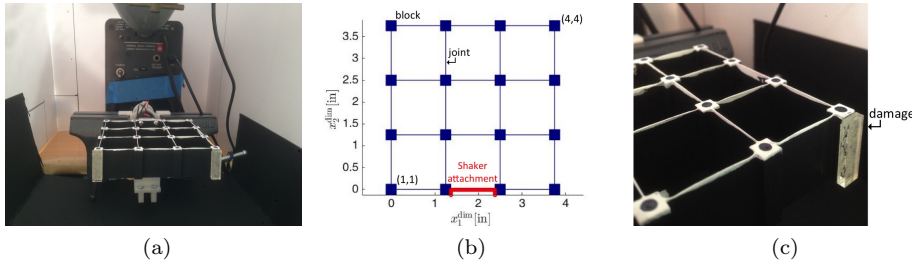


Fig. 1: Microtruss experiment. Figure (a): experimental apparatus. Figure (b): schematic of undamaged configuration at rest. Figure (c): detail of the added mass on top of block (1, 4).

where $V_{\text{nom}} = h \ell_{\text{block}} d_{\text{mtruss}}$, $h = \frac{1}{2}(d_{\text{block}} - h_{\text{joint}})$, is a nominal volume, V_{left} is the volume of the added mass on top of block (1, 4), and V_{right} is the volume of the added mass on top of block (4, 4). We observe that the ratios in (1) do not rely on any model of the structure.

We can now introduce the function $\bar{f}^{\text{dam}} : [1, 2]^2 \rightarrow \{1, 2, 3, 4\}$ such that

$$\bar{f}^{\text{dam}}(s_L, s_R) = \begin{cases} 1 & s_L, s_R \leq 1.5, \\ 2 & s_L > 1.5, s_R \leq 1.5, \\ 3 & s_L \leq 1.5, s_R > 1.5, \\ 4 & s_L, s_R > 1.5. \end{cases} \quad (2)$$

The function \bar{f}^{dam} reflects our actionable definition of damage for the structure of interest; given the system configuration described by the pair (s_L, s_R) , $y = \bar{f}^{\text{dam}}(s_L, s_R)$ denotes the corresponding state of damage. For this reason, we refer to \bar{f}^{dam} as the *damage function*. From an engineering perspective, equation (2) implies that system configurations should be classified as damaged only if the added mass is “substantial”, in our case of volume larger than $0.5V_{\text{nom}} \approx 0.37 \cdot 10^{-3}[\text{in}^3]$. We remark that, from a practical perspective, the proper choice of the threshold is extremely important and should be related to appropriate safety factors ([71]). In section 2.6 we shall provide a general form for the damage function in terms of the system configuration.

2.3 Data acquisition and experimental outputs

We rely on a camera to acquire measurements of the x_2 displacement of the 16 respective centers of the blocks as a function of time t associated with Q_1 different time-harmonic inputs. The camera is carefully calibrated to permit its use for precise measurement. A stroboscope flashing at the 10 Hz frame rate of the camera “freezes” the oscillation of the blocks to yield crisp images suitable for subsequent processing. Frequencies of excitation are offset by 0.1 Hz from integer values to ensure that each set of 100 consecutively captured images corresponds to 100 equally spaced instants in a single period of oscillation.

Excitations are imposed by a linear voice coil actuator attached to the joint between blocks (2, 1) and (3, 1); Figure 1(b) highlights in red the region of the microtruss attached to the actuator. A linear flexure bearing is used to ensure that the excitation is imposed almost exclusively in the x_2 direction.

We introduce the system configuration \mathcal{C} associated with the particular specimen considered; we defer the formal definition of \mathcal{C} to section 2.4. Then, we denote by $\{f^q\}_{q=1}^{Q_1} \subset \mathcal{I}_f := [20, 80][\text{Hz}]$ the input frequencies and we denote by $\{q_{i,j}^{\text{exp}}(t^\ell, f^q; \mathcal{C})\}_{\ell=1}^L$ the raw time signal for the x_2 -displacement obtained experimentally for the block (i, j) and the frequency f^q . Finally, we introduce the fitted amplitude $\{\bar{A}_{i,j}^{\text{exp}}(f^q; \mathcal{C})\}_{i,j,q}$ and phase $\{\bar{\phi}_{i,j}^{\text{exp}}(f^q; \mathcal{C})\}_{i,j,q}$ such that¹

$$q_{i,j}^{\text{exp}}(t^\ell, f^q; \mathcal{C}) \approx \bar{A}_{i,j}^{\text{exp}}(f^q; \mathcal{C}) \cos\left(2\pi f^q t^\ell + \bar{\phi}_{i,j}^{\text{exp}}(f^q; \mathcal{C})\right), \quad i, j = 1, \dots, 4, \ell = 1, \dots, L. \quad (3)$$

It is convenient to rescale amplitudes and phases as follows:

$$A_{i,j}^{\text{exp}}(f^q; \mathcal{C}) := \frac{A_{\text{nom}}}{\bar{A}_{2,1}^{\text{exp}}(f^q; \mathcal{C})} \bar{A}_{i,j}^{\text{exp}}(f^q; \mathcal{C}), \quad \phi_{i,j}^{\text{exp}}(f^q; \mathcal{C}) = \bar{\phi}_{i,j}^{\text{exp}}(f^q; \mathcal{C}) - \bar{\phi}_{2,1}^{\text{exp}}(f^q; \mathcal{C}), \quad (4)$$

for $A_{\text{nom}} = 0.25$. Figure 2 demonstrates the accuracy of the time-harmonic fit for the blocks (1, 4) and (4, 4) in absence of added masses. In section 2.4, we describe how we shall estimate $\{A_{i,j}^{\text{exp}}(f^q; \mathcal{C})\}$ and $\{\phi_{i,j}^{\text{exp}}(f^q; \mathcal{C})\}$ based on simulations.

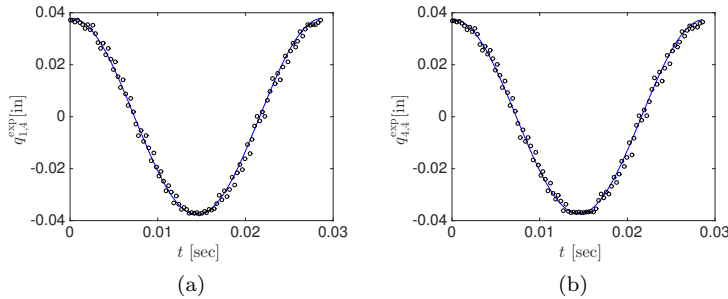


Fig. 2: Microtruss experiment. Time-harmonic x_2 -displacement of blocks (1, 4) and (4, 4) in absence of added masses. The shaker input is displacement: $A^{\text{dim}} \cos(2\pi f t) \mathbf{e}_2$, $A^{\text{dim}} = 0.02[\text{in}]$, $f = 35 [\text{Hz}]$.

¹ Amplitudes and phases are estimated using the Matlab function `fit` ([43]), which relies on Levenberg-Marquardt algorithm.

2.4 Mathematical model for the experimental outputs

We first provide a mathematical description of the nominal geometry at rest. With this in mind, we introduce the disjoint domains $\Omega_1, \Omega_2, \Omega_3 \subset \Omega$, $\overline{\Omega_1} \cup \overline{\Omega_2} \cup \overline{\Omega_3} = \overline{\Omega}$. The subdomain Ω_2 is associated with the region of block (1, 4) subject to potential damage; similarly, the subdomain Ω_3 is associated with the region of block (4, 4), while Ω_1 denotes the remainder of the microtruss. We then recall the geometric parameters $s_L, s_R \in [1, 2]$ in (1) such that $(s_L - 1)V_{\text{nom}}$ and $(s_R - 1)V_{\text{nom}}$ correspond to the volume of the added masses on top of blocks (1, 4) and (4, 4), respectively. Assuming that the depth of the blocks is uniformly equal to d_{mtruss} and the width of the block is uniformly equal to ℓ_{block} , then we have that $(s_L - 1)h$ and $(s_R - 1)h$ equal the thickness of the added masses on top of (1, 4) and (4, 4), respectively. Figure 3 shows blocks (1, 4) and (4, 4) and provides a graphical depiction of the previous definitions. In what follows, we denote by Ω_s the domain $\Omega_s = \Omega_1 \cup \Omega_2(s_L) \cup \Omega_3(s_R)$.

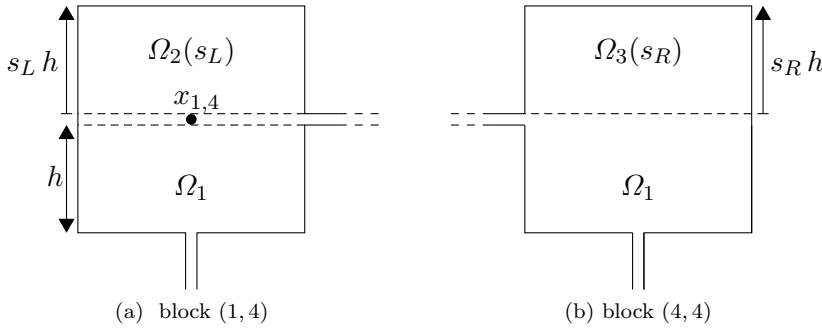


Fig. 3: Microtruss experiment. Parametrization of blocks (1, 4) and (4, 4).

We can now introduce the mathematical model of the displacement field in strong form. With this in mind, we introduce the Young's modulus $E[\text{Pa}]$, the Poisson's ratio ν , the density $\rho[\text{kg}/\text{m}^3]$, and the non-dimensional Rayleigh-damping coefficients α, β . For acrylic, density and Poisson's ratio are well-characterized in the literature²: we therefore set

$$\rho = 1180 [\text{kg}/\text{m}^3], \quad \nu = 0.35.$$

On the other hand, we consider α, β, E as uncertain parameters. We assume that the (non-dimensional) displacement field associated with the microtruss system is of the form $U^{\text{bk}}(x, t) = \Re\{u^{\text{bk}}(x) e^{i\omega_f t}\}$ where $\omega_f = 2\pi f$ and $u^{\text{bk}} : \Omega_s \rightarrow \mathbb{C}^2$ satisfies (in a distributional sense) the following linear two-

² See, e.g., [30, Chapter 3.6.2] for the Poisson's ratio and the webpage pubchem.ncbi.nlm.nih.gov for the density.

dimensional (plane strain) elastodynamics model with Rayleigh damping:

$$\begin{cases} -\rho L_{\text{joint}}^2 \omega_f^2 u^{\text{bk}} + i\omega_f \mathcal{C}^{\text{damp}}(u^{\text{bk}}) + \mathcal{L}(u^{\text{bk}}) = 0 & \text{in } \Omega_s, \\ u^{\text{bk}} = u^{\text{dir}} & \text{on } \Gamma^{\text{dir}}, \\ \sigma(u^{\text{bk}}) \cdot \mathbf{n} = 0 & \text{on } \partial\Omega_s \setminus \Gamma^{\text{dir}}, \end{cases} \quad (5a)$$

where Γ^{dir} refers to the shaker attachment, $\sigma(u^{\text{bk}})$ is the stress tensor, and \mathbf{n} is the outward normal. Here, the Dirichlet data is

$$u^{\text{dir}} = c^{\text{dir}} \begin{bmatrix} 0 \\ 1 \end{bmatrix}, \quad (5b)$$

the damping operator is

$$\mathcal{C}^{\text{damp}}(v) = \alpha \rho L_{\text{joint}}^2 v + \beta \mathcal{L}(v), \quad (5c)$$

and finally the elasticity operator $\mathcal{L}(v) = \text{div}(\sigma(v))$ is

$$\mathcal{L}(v) = \text{div} \left(\frac{E}{1+\nu} \text{sym}(\nabla v) + \frac{E\nu}{(1+\nu)(1-2\nu)} \text{div}(v)\mathbb{I} \right), \quad (5d)$$

where \mathbb{I} is the 2 by 2 identity matrix. Recalling the definition of the experimental outputs in (4), it is easy to verify that the constant c^{dir} does not influence the outputs. For this reason, we arbitrarily set $c^{\text{dir}} = 1$.

We now introduce the anticipated configuration μ as

$$\mu = [\alpha, \beta, E, s_L, s_R] \in \mathcal{P}^{\text{bk}} \subset \mathbb{R}^5. \quad (6)$$

We observe that the solution u^{bk} to (5) depends on the input frequency f and on μ , which we shall emphasize in the notation $u^{\text{bk}} = u^{\text{bk}}(f; \mu)$. We further observe that the pair (s_L, s_R) is directly related to the definition of damage in (15), while the triplet (α, β, E) collects material properties that are difficult to estimate exactly. We postpone the definition of the configuration set \mathcal{P}^{bk} to the end of this section.

We observe that our mathematical model does not include some factors that may affect the experimental outputs. More in detail, we do not take into account potential inaccuracies in the manufacturing process, which lead to extremely high-dimensional geometric uncertainties, or to inhomogeneities in the material properties. Furthermore, we do not prescribe a stochastic model for experimental noise. In anticipation of the development of a rigorous mathematical formulation of the inference problem, we introduce an additional set of parameters $\xi \in \mathcal{V} \subset \mathbb{R}^D$, here referred to as *hidden*, such that the pair (μ, ξ) completely identifies a system configuration:

$$\mathcal{C} := (\mu, \xi) \in \mathcal{P}^{\text{exp}} := \mathcal{P}^{\text{bk}} \times \mathcal{V}. \quad (7)$$

Our best-knowledge model corresponds to $\xi = 0$.

We can now introduce the best-knowledge representation of the experimental outputs $A_{i,j}^{\text{exp}}$ and $\phi_{i,j}^{\text{exp}}$. Given the anticipated configuration $\mu \in \mathcal{P}^{\text{bk}}$, we define

$$A_{i,j}^{\text{bk}}(f; \mu) := \frac{A_{\text{nom}}}{|u_2^{\text{bk}}(x_{2,1}; f; \mu)|} |u_2^{\text{bk}}(x_{i,j}; f; \mu)|, \quad A_{\text{nom}} = 0.25, \quad (8)$$

and

$$\phi_{i,j}^{\text{bk}}(f; \mu) := \arg(u_2^{\text{bk}}(x_{i,j}; f; \mu)) - \arg(u_2^{\text{bk}}(x_{2,1}; f; \mu)), \quad (9)$$

where $x_{i,j}$ denotes the center of the mass (i, j) and $\arg(c)$ denotes the phase of the complex number c . As stated before, the best-knowledge outputs considered do not depend on the value of c^{dir} in (5b). Provided that the linear model (5) captures accurately the physical phenomenon and the influence of the hidden parameter ξ is limited, we expect that

$$A_{i,j}^{\text{exp}}(f; \mu, \xi) \simeq A_{i,j}^{\text{bk}}(f; \mu), \quad \phi_{i,j}^{\text{exp}}(f; \mu, \xi) \simeq \phi_{i,j}^{\text{bk}}(f; \mu),$$

for all $f \in \mathcal{I}_f$, $\mu \in \mathcal{P}^{\text{bk}}$ and $i, j = 1, \dots, 4$.

We rely on a P4 Finite Element (FE) discretization with 14670 degrees of freedom to estimate the best-knowledge outputs. We observe that experimental outputs involve pointwise evaluations of the displacement field. In this work, we do not implement any adaptive strategy to control pointwise error in the finite element solution; we refer to the finite element literature (see, e.g., [48]) for further details.

We now choose the anticipated configuration set \mathcal{P}^{bk} . Towards this end, we consider a single preliminary experiment for the undamaged case (i.e., $s_L = s_R = 1$). To take into account experimental noise, we perform three independent trials of the experiment. Then, we choose \mathcal{P}^{bk} such that for all frequencies and all realizations we obtain

$$\min_{\mu \in \Xi_{100}} A_{i,j}^{\text{bk}}(f^q; \mu) < A_{i,j}^{\text{exp}}(f^q; \mu^{\text{exp}}, \xi^{\text{exp}}) < \max_{\mu \in \Xi_{100}} A_{i,j}^{\text{bk}}(f^q; \mu), \quad (10a)$$

and

$$\min_{\mu \in \Xi_{100}} \phi_{i,j}^{\text{bk}}(f^q; \mu) < \phi_{i,j}^{\text{exp}}(f^q; \mu^{\text{exp}}, \xi^{\text{exp}}) < \max_{\mu \in \Xi_{100}} \phi_{i,j}^{\text{bk}}(f^q; \mu), \quad (10b)$$

where $\Xi_{100} = \{(\alpha^m, \beta^m, E^m, 1, 1)\}_{m=1}^M \subset \mathcal{P}^{\text{bk}}$ is based on uniform random samples. Following this criterion, we choose

$$\mathcal{P}^{\text{bk}} := [0.25 \cdot 10^{-3}, 0.8 \cdot 10^{-3}] \times [0.05 \cdot 10^{-3}, 0.2 \cdot 10^{-3}] \times [2.65 \cdot 10^9, 2.85 \cdot 10^9] \times [1, 2]^2. \quad (11)$$

Figure 4 shows a comparison between experimental and synthetic displacement amplitudes of block (1, 1) for this single system configuration with no added masses. In Figure 4(a), we report $\min_{\mu \in \Xi_{100}} A_{1,1}^{\text{bk}}(f^q; \mu)$, $\max_{\mu \in \Xi_{100}} A_{1,1}^{\text{bk}}(f^q; \mu)$, and the amplitude measured experimentally for each of the three trials. Similarly, in Figure 4(b), we report $\min_{\mu \in \Xi_{100}} \phi_{1,1}^{\text{bk}}(f^q; \mu)$, $\max_{\mu \in \Xi_{100}} \phi_{1,1}^{\text{bk}}(f^q; \mu)$ and the phase measured experimentally for each trial. We observe that our choice (11) satisfies the constraints (10).

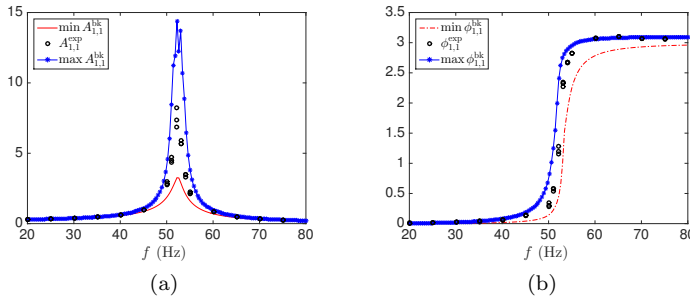


Fig. 4: Microtruss experiment; choice of the parameter space. Comparison between experimental results and synthetic results in absence of added masses.

2.5 The problem of feature extraction

We formalize the problem of feature extraction for the microtruss system: given the experimental outputs $\{A_{i,j}^{\text{exp}}(f^q; \mu, \xi)\}_{i,j,q}$ and $\{\phi_{i,j}^{\text{exp}}(f^q; \mu, \xi)\}_{i,j,q}$, determine the set of Q features \mathbf{z}^{exp} such that

$$\mathbf{z}^{\text{exp}}(\mu, \xi) = \mathcal{F}(\{A_{i,j}^{\text{exp}}(f^q; \mu, \xi)\}_{i,j,q}, \{\phi_{i,j}^{\text{exp}}(f^q; \mu, \xi)\}_{i,j,q}), \quad (12)$$

where $\mathcal{F} : \mathbb{R}^{32Q_1} \rightarrow \mathbb{R}^Q$. We observe that, by construction, experimental features depend on the system configuration $\mathcal{C} = (\mu, \xi)$. Appropriate features should be sensitive to the expected damage, and insensitive to noise. In section 4.1, we propose a particular choice of \mathcal{F} motivated by a physical reasoning for our system and damage classes. We defer automated identification of features from experimental outputs to a subsequent paper.

Exploiting the best-knowledge representations of the experimental outputs provided in section 2.4, we can define the best-knowledge features as

$$\mathbf{z}^{\text{bk}}(\mu) = \mathcal{F}(\{A_{i,j}^{\text{bk}}(f^q; \mu)\}_{i,j,q}, \{\phi_{i,j}^{\text{bk}}(f^q; \mu)\}_{i,j,q}). \quad (13)$$

We observe that, without loss of generality, we can rewrite the experimental features as

$$\mathbf{z}^{\text{exp}}(\mu, \xi) = \mathbf{z}^{\text{bk}}(\mu) + \delta\mathbf{z}(\mu, \xi), \quad \forall (\mu, \xi) \in \mathcal{P}^{\text{exp}}; \quad (14)$$

we can then interpret $\mathbf{z}^{\text{bk}}(\mu)$ as *nominal features* associated with the configuration $\mathcal{C} = (\mu, \xi)$, and $\delta\mathbf{z}(\mu, \xi)$ as a perturbation. The norm $\|\delta\mathbf{z}(\mu, \xi)\|_2$ reflects the magnitude of the model error for a given configuration. We anticipate that (14) will help us draw a connection between our formulation and Robust Optimization (RO) statements for classification.

2.6 Inference stage

We summarise key quantities introduced in the previous sections. We first define the anticipated configuration set $\mathcal{P}^{\text{bk}} \subset \mathbb{R}^P$, and we denote by μ a

generic element of the set. The parameter μ encodes our best-knowledge (bk) representation of a system configuration and the space \mathcal{P}^{bk} contains the bk anticipation of each system configuration that can occur during the operations (online stage). We further introduce the hidden parameter $\xi \in \mathcal{V} \subset \mathbb{R}^D$ such that the pair $\mathcal{C} = (\mu, \xi) \in \mathcal{P}^{\text{exp}} := \mathcal{P}^{\text{bk}} \times \mathcal{V}$ uniquely identifies the observed experimental outputs during the online stage. Then, we introduce the damage function $f^{\text{dam}} : \mathcal{P}^{\text{bk}} \rightarrow \{1, \dots, K\}$ such that

$$f^{\text{dam}}(\mu = [\alpha, \beta, E, s_L, s_R]) = \bar{f}^{\text{dam}}(s_L, s_R), \quad (15)$$

where \bar{f}^{dam} is defined in (2). We observe that the actual value of the model parameters α, β, E does not influence the state of damage. We can thus interpret them as nuisance variables. We further introduce the bk and experimental features $\mathbf{z}^{\text{bk}} : \mathcal{P}^{\text{bk}} \rightarrow \mathbb{R}^Q$ and $\mathbf{z}^{\text{exp}} : \mathcal{P}^{\text{exp}} \rightarrow \mathbb{R}^Q$, respectively.

In view of the classification statement, we introduce the (unknown) probability density function (pdf) over \mathcal{V} , $p_\xi : \mathcal{V} \rightarrow \mathbb{R}_+$, such that

$$P(\xi \in A) = \int_{\mathcal{V}} \mathbb{1}_A(\xi') p_\xi(\xi') d\xi', \quad A \subset \mathcal{V}, \quad (16)$$

where $\mathbb{1}_A$ is the indicator function associated to the set A . We use notation $\mathbb{E}_{\xi \sim p_\xi}[\cdot]$ to indicate expected values with respect to the measure induced by p_ξ . We further denote by $\mathcal{L}^{(0,1)}$ the 0-1 loss:

$$\mathcal{L}^{(0,1)}(y, t) = \begin{cases} 0 & y = t, \\ 1 & y \neq t. \end{cases} \quad (17)$$

Finally, we define the weight $w^{\text{bk}}, w^{\text{bk}} : \mathcal{P}^{\text{bk}} \rightarrow \mathbb{R}_+$, such that

$$\int_{\mathcal{P}^{\text{bk}}} w^{\text{bk}}(\mu) d\mu = 1. \quad (18)$$

We postpone interpretation and actionable definition of the weight w^{bk} until the end of this section.

We now introduce two classification problem statements.

Monitoring problem: given the damage function $f^{\text{dam}} : \mathcal{P}^{\text{bk}} \rightarrow \{1, \dots, K\}$, and the experimental features $\mathbf{z}^{\text{exp}} : \mathcal{P}^{\text{exp}} \rightarrow \mathbb{R}^Q$, find the classifier $g^{\text{opt}} : \mathbb{R}^Q \rightarrow \{1, \dots, K\}$ that minimizes the *experimental risk*:

$$\begin{aligned} \inf_{g \text{ measurable}} R^{\text{exp}}(g) &= \int_{\mathcal{P}^{\text{bk}}} \mathbb{E}_{\xi \sim p_\xi} \left[\mathcal{L}^{(0,1)}(g(\mathbf{z}^{\text{exp}}(\mu, \xi)), f^{\text{dam}}(\mu)) \right] w^{\text{bk}}(\mu) d\mu \\ &= \int_{\mathcal{P}^{\text{exp}}} \mathcal{L}^{(0,1)}(g(\mathbf{z}^{\text{exp}}(\mu, \xi)), f^{\text{dam}}(\mu)) w^{\text{bk}}(\mu) p_\xi(\xi) d\mu d\xi, \end{aligned} \quad (19)$$

where $p_\xi : \mathcal{V} \rightarrow \mathbb{R}_+$ is defined in (16), $\mathcal{L}^{(0,1)}$ in (17), and $w^{\text{bk}} : \mathcal{P}^{\text{bk}} \rightarrow \mathbb{R}_+$ in (18).

Best-knowledge monitoring problem: given the damage function $f^{\text{dam}} : \mathcal{P}^{\text{bk}} \rightarrow \{1, \dots, K\}$, and the bk features $\mathbf{z}^{\text{bk}} : \mathcal{P}^{\text{bk}} \rightarrow \mathbb{R}^Q$, find the classifier $g^{\text{opt,bk}} : \mathbb{R}^Q \rightarrow \{1, \dots, K\}$ that minimizes the *bk risk*:

$$\inf_{g \text{ measurable}} R^{\text{bk}}(g) = \int_{\mathcal{P}^{\text{bk}}} \mathcal{L}^{(0,1)}(g(\mathbf{z}^{\text{bk}}(\mu)), f^{\text{dam}}(\mu)) w^{\text{bk}}(\mu) d\mu. \quad (20)$$

where $\mathcal{L}^{(0,1)}$ is defined in (17), and $w^{\text{bk}} : \mathcal{P}^{\text{bk}} \rightarrow \mathbb{R}_+$ (18).

We interpret the bk monitoring problem as a surrogate for the (actual, physical) monitoring problem. We observe that while the monitoring statement relies on experimental observations and depends on unknown quantities (the hidden parameter ξ and the corresponding pdf p_ξ), the bk statement is entirely synthetic and thus can be tackled even in the absence of experimental observations. At this stage of the discussion, we have not yet discussed how the solution to (20) is related to the optimal solution to (19). This clearly depends on the magnitude of the perturbations $\delta \mathbf{z}$ in (14). In section 5, we illustrate the connection between these two problems.

We now interpret the function w^{bk} in (19) and (20). In our framework, the weight w^{bk} reflects the importance (assigned by the user) of classifying correctly a given configuration and is not related to the (unknown) likelihood that the bk configuration μ is observed during the online stage. This observation implies that the bk risk $R^{\text{bk}}(g)$ should be interpreted as a user-defined measure of the misclassification error rather than an expected loss.

We introduce our choice of the weight w^{bk} for the microtruss problem. We consider the weight

$$w^{\text{bk}}(\mu) = w_1^{\text{bk}}(\alpha) w_2^{\text{bk}}(\beta) w_3^{\text{bk}}(E) w_{4,5}^{\text{bk}}(s_L, s_R), \quad (21a)$$

where $w_1^{\text{bk}}, w_2^{\text{bk}}, w_3^{\text{bk}}$ correspond to constant weights and

$$w_{4,5}^{\text{bk}}(s_L, s_R) = \begin{cases} 100 & (s_L, s_R) \in S_1 := [1, 1.05]^2; \\ 10 & (s_L, s_R) \in S_2 := [1.5, 2] \times [1, 1.05]; \\ 10 & (s_L, s_R) \in S_3 := [1, 1.05] \times [1.5, 2]; \\ 1 & (s_L, s_R) \in S_4 := [1.5, 2]^2. \end{cases} \quad (21b)$$

We choose constants such that $\int_{\mathcal{P}^{\text{bk}}} w^{\text{bk}}(\mu) d\mu = 1$. We observe that each of S_1, \dots, S_4 are assigned equal weight.

Some comments are in order. Our choice of $w_{4,5}^{\text{bk}}$ in (21b) implies that we target our SHM classifier to detect added masses in the range $[1.5, 2]h$, and to avoid “false damaged” predictions if $s_L, s_R < 1.05$. In view of the probabilistic interpretation of the problem statement and of the numerical procedure, we observe that our choices of $w_1^{\text{bk}}, w_2^{\text{bk}}, w_3^{\text{bk}}$ correspond to the assumption that

α, β, E are independent uniformly-distributed random variables such that

$$\begin{aligned}\alpha &\sim \text{Uniform}([0.25 \cdot 10^{-3}, 0.8 \cdot 10^{-3}]), \\ \beta &\sim \text{Uniform}([0.05 \cdot 10^{-3}, 0.2 \cdot 10^{-3}]), \\ E &\sim \text{Uniform}([2.65 \cdot 10^9, 2.85 \cdot 10^9]).\end{aligned}\tag{22a}$$

On the other hand, our choice of $w_{4,5}^{\text{bk}}$ corresponds to assume that the random pair (s_L, s_R) can be written as a mixture of independent uniform distributions over S_1, \dots, S_4 :

$$(s_L, s_R) = \sum_{k=1}^4 \left(1 - \mathcal{L}^{(0,1)}(S, k)\right) E_k, \quad E_k \sim \text{Uniform}(S_k), \quad S \sim \text{Uniform}(\{1, 2, 3, 4\}).\tag{22b}$$

We shall later formally identify w^{bk} with a probability density. Table 1 summarizes the definitions and provides links to their instantiations for the microtruss problem.

Table 1: Main definitions

symbol	name	microtruss definition
$\mu \in \mathcal{P}^{\text{bk}}$	anticipated configuration (set)	(6) – (11)
$(\mu, \xi) \in \mathcal{P}^{\text{exp}}$	configuration (set)	(7)
$f^{\text{dam}} : \mathcal{P}^{\text{bk}} \rightarrow \{1, \dots, K\}$	damage function	(15)
$\mathbf{z}^{\text{exp}} : \mathcal{P}^{\text{exp}} \rightarrow \mathbb{R}^{\mathcal{Q}}$	experimental features	(12)
$\mathbf{z}^{\text{bk}} : \mathcal{P}^{\text{bk}} \rightarrow \mathbb{R}^{\mathcal{Q}}$	bk features	(13)
$w^{\text{bk}} : \mathcal{P}^{\text{bk}} \rightarrow \mathbb{R}_+$	bk weight	(21)

Before concluding, we state another definition, and an important remark.

Definition 1 Let us define the partition of the configuration set $\{\mathcal{P}^{\text{bk}}(k)\}_{k=1}^K$ as

$$\mathcal{P}^{\text{bk}}(k) := \{\mu \in \mathcal{P}^{\text{bk}} : f^{\text{dam}}(\mu) = k\}, \quad k = 1, \dots, K.$$

Then, we define the type- k error of a classifier g as

$$R^{\text{exp}}(g; k) := \int_{\mathcal{P}^{\text{bk}}(k) \times \mathcal{V}} \mathbb{E}_{\xi \sim p_\xi} \left[\mathcal{L}^{(0,1)}(g(\mathbf{z}^{\text{exp}}(\mu, \xi)), k) \right] w^{\text{bk}}(\mu) d\mu; \tag{23}$$

similarly, we can define the bk-type- k error as

$$R^{\text{bk}}(g; k) := \int_{\mathcal{P}^{\text{bk}}(k)} \mathcal{L}^{(0,1)}(g(\mathbf{z}^{\text{bk}}(\mu)), k) w^{\text{bk}}(\mu) d\mu. \tag{24}$$

If $K = 2$, provided that $y = 1$ is the null hypothesis, our definition of type- k error coincides with the standard type I and type II errors in Hypothesis Testing.

It is straightforward to verify that

$$R^{\text{bk}}(g) = \sum_{k=1}^K R^{\text{bk}}(g; k), \quad R^{\text{exp}}(g) = \sum_{k=1}^K R^{\text{exp}}(g; k).$$

We observe that if we define the bk confusion matrix $\mathbb{C}^{\text{bk}}(g) \in \mathbb{R}^{K,K}$ associated with the classifier g such that

$$\mathbb{C}_{k,k'}^{\text{bk}}(g) = \int_{\mathcal{P}^{\text{bk}}(k)} \mathcal{L}^{(0,1)}(g(\mathbf{z}^{\text{bk}}(\mu)), k') w^{\text{bk}}(\mu) d\mu,$$

then, the bk type- k error is the sum of the off-diagonal terms of $\mathbb{C}^{\text{bk}}(g)$:

$$R^{\text{bk}}(g, k) = \sum_{k' \neq k} \mathbb{C}_{k,k'}^{\text{bk}}(g).$$

An analogous discussion applies to the type- k error. We further observe that the choice of w^{bk} regulates the importance of the different types of error. More specifically, for each k , we can interpret the quantity

$$P_k^{\text{bk}} := \int_{\mathcal{P}^{\text{bk}}(k)} w^{\text{bk}}(\mu) d\mu \quad (25)$$

as a measure of the importance of classifying correctly configurations of class k . For the microtruss problem, we have

$$P_1^{\text{bk}} = \dots = P_4^{\text{bk}} = \frac{1}{4}.$$

This implies that it is equally important to classify correctly configurations of all four classes.

Remark 1 (The perspective of Robust Optimization) Adopting the interpretation of bk and experimental features provided after equation (14), we can view (20) as the *nominal problem*, and (19) as the *perturbed problem*. This discussion shows the connection between our formulation and Robust Optimization (RO) statements for classification. To stress this, we observe that we can restate the experimental risk in (19) as follows:

$$R^{\text{exp}}(g) = \int_{\mathcal{P}^{\text{bk}}} \mathbb{E}_{\delta \mathbf{z} \sim P_{\delta \mathbf{z}, \mu}} \left[\mathcal{L}^{(0,1)}(g(\mathbf{z}^{\text{bk}}(\mu) + \delta \mathbf{z}), f^{\text{dam}}(\mu)) \right] w^{\text{bk}}(\mu) d\mu, \quad (26)$$

where the probability distribution $P_{\delta \mathbf{z}, \mu}$ is given by

$$P_{\delta \mathbf{z}, \mu}(A) = \int_{\mathcal{V}} \mathbb{1}_A(\delta \mathbf{z}(\mu, \xi)) p_{\xi}(\xi) d\xi, \quad (27)$$

and is defined over (a suitable σ -algebra of) \mathbb{R}^Q .

3 Methodology

We discuss here how we estimate the solution to (20). We first present the general computational procedure (section 3.1), and we then discuss the application of pMOR (section 3.2).

3.1 Simulation-based classification

In view of the development of the computational approach, we define the probability measure on \mathcal{P}^{bk} $P_{w^{\text{bk}}}$ such that

$$P_{w^{\text{bk}}}(A) = \int_{\mathcal{P}^{\text{bk}}} \mathbb{1}_A(\mu') w^{\text{bk}}(\mu') d\mu', \quad A \subset \mathcal{P}^{\text{bk}}. \quad (28)$$

Then, we denote by μ a random vector distributed according to $P_{w^{\text{bk}}}$, $\mu \sim P_{w^{\text{bk}}}$.

We formalize our strategy to generate the classifier g . We generate M independent samples μ^1, \dots, μ^M from $P_{w^{\text{bk}}}$, and we generate the dataset $\mathcal{D}_M^{\text{bk}} := \{(\mathbf{z}^{\text{bk},m}, y^m)\}_{m=1}^M$ where $\mathbf{z}^{\text{bk},m} = \mathbf{z}^{\text{bk}}(\mu^m)$, $y^m = f^{\text{dam}}(\mu^m)$. Then, we employ a supervised learning algorithm that takes as input the dataset $\mathcal{D}_M^{\text{bk}}$ and returns the classifier g_M^* .

Several techniques are available to generate independent samples from an arbitrary probability density function w^{bk} . We refer to [53, Chapter 2] and to [27, Chapter 3] for further details. Here, we resort to identities (22) to generate samples of the configuration μ .

A supervised learning (SL) algorithm for classification can be interpreted as a procedure that takes as input a dataset $\mathcal{D}_M^{\text{bk}} \subset \mathbb{R}^Q \times \{1, \dots, K\}$ and returns a classifier $g_M^* : \mathbb{R}^Q \rightarrow \{1, \dots, K\}$:

$$[g_M^*] = \text{SL-algorithm}(\mathcal{D}_M^{\text{bk}}). \quad (29)$$

Several different algorithms of the form (29) have been proposed in the literature; we refer to [31, 38, 45] for a thorough introduction to supervised learning algorithms for regression and classification. In our numerical examples, we apply five different state-of-the-art techniques to the classification problem considered in this work.

Algorithm 1 summarizes the computational procedure to approximate the solution to the best-knowledge monitoring problem: both the Offline stage described above; the Online stage in which, given experimental features, we wish to classify our system.

Algorithm 1 Simulation-Based Classification for SHM.**Offline stage**

- 1: Generate $\mathcal{P}_M^{\text{bk}} := \{\mu^1, \dots, \mu^M\} \subset \mathcal{P}^{\text{bk}}$, $\mu^m \stackrel{iid}{\sim} P_{w^{\text{bk}}}$
- 2: Generate the dataset $\mathcal{D}_M^{\text{bk}} := \{(\mathbf{z}^{\text{bk},m}, y^m)\}_{m=1}^M$ where $\mathbf{z}^{\text{bk},m} = \mathbf{z}^{\text{bk}}(\mu^m)$, $y^m = f^{\text{dam}}(\mu^m)$.
- 3: Employ the learning algorithm (29) to generate the classifier g_M^* .

Online stage

- 1: Collect the experimental measurements and extract the features \mathbf{z}^{exp} .
- 2: Return the label $g_M^*(\mathbf{z}^{\text{exp}})$.

We observe that, unlike in model-based approaches, our procedure does not — either implicitly or explicitly — provide estimates for the actual value of μ . We argue that this is the main advantage of simulation-based approaches compared to model-based approaches since the estimation of μ is a much more general problem than the original classification problem and thus is more likely to be ill-posed ([65, Chapter 1.9]). For instance, the application of model-based approaches to the microtruss problem requires the estimate of the full vector μ , which includes both quantities related to damage (the geometric parameters s_L, s_R) but also nuisance variables (the material properties α, β, E).

Another distinguishing feature of Simulation-Based Classification is related to the possibility of incorporating information related to model error without the need for fully characterizing the configuration $\mathcal{C} = (\mu, \xi)$. We can indeed include estimates of the perturbation $\delta\mathbf{z}$ to inform the learning procedure. The process of including data uncertainties at training stage is usually referred to as *robustification*. We shall consider this in future work.

3.2 Application of pMOR

As already mentioned in the introduction, classification performances strongly depend on the size M of the dataset. Since each datapoint involves the solution to several PDEs (in our case Q_1 , one for each frequency), the offline computational burden is extremely large. This explains the importance of model order reduction.

We briefly discuss the application of pMOR in the context of Simulation-Based Classification. During a preprocessing stage (typically denoted the offline stage), we generate a Reduced Order Model (ROM) $\tilde{u}^{\text{bk}}(f; \mu) \approx u^{\text{bk}}(f; \mu)$ such that we may form $\tilde{\mathbf{z}}^{\text{bk}}(\mu) \approx \mathbf{z}^{\text{bk}}(\mu)$ for all $\mu \in \mathcal{P}^{\text{bk}}$. Then, for each parameter μ^1, \dots, μ^M , we estimate $\mathbf{z}^{\text{bk}}(\mu^m)$ using the ROM $\tilde{\mathbf{z}}^{\text{bk}}(\mu^m)$. We observe that if M is sufficiently large and computing $\tilde{\mathbf{z}}^{\text{bk}}(\mu^m)$ is significantly less expensive than computing $\mathbf{z}^{\text{bk}}(\mu^m)$, then we can amortize and indeed neglect the cost of the preprocessing stage.

Algorithm 2 summarizes the computational procedure. Note that both the offline stage and the online stage of the pMOR procedure are effected in the offline stage of the classification algorithm. We provide further details about the application of the particular pMOR technique adopted in this paper to the microtruss problem in section 4.3.

Algorithm 2 Simulation-Based Classification for SHM with pMOR.

Offline stage

- 1: Generate $\mathcal{P}_M^{\text{bk}} := \{\mu^1, \dots, \mu^M\} \subset \mathcal{P}^{\text{bk}}, \mu^m \overset{iid}{\sim} P_{w^{\text{bk}}}$
- 2: a. MOR: construct the Reduced Order Model;
b. MOR: use the ROM to generate the dataset $\mathcal{D}_M^{\text{bk}} := \{(\tilde{\mathbf{z}}^{\text{bk}}(\mu^m), f^{\text{dam}}(\mu^m))\}_{m=1}^M$
- 3: Employ the learning algorithm (29) to generate the classifier g_M^* .

Online stage

- 1: Collect the experimental measurements and extract the features \mathbf{z}^{exp} .
 - 2: Return the label $g_M^*(\mathbf{z}^{\text{exp}})$.
-

4 Application to the microtruss problem

We discuss the application of Simulation-Based Classification to the microtruss problem. We discuss the choice of the features (section 4.1), we present the strategy used to generate the classifier (section 4.2), and we describe the application of the RB method to speed up the calculations (section 4.3). Finally, in section 4.4, we present the classification results.

4.1 Feature extraction

Given the frequencies $\{f^q\}_{q=1}^{Q_1}$, we introduce the set of features

$$\mathbf{z}_1^{\text{bk}}(\mu) = [z_1^{\text{bk}}(f^1; \mu), \dots, z_1^{\text{bk}}(f^{Q_1}; \mu)], \quad z_1^{\text{bk}}(f; \mu) = \frac{A_{1,4}^{\text{bk}}(f; \mu)}{A_{4,4}^{\text{bk}}(f; \mu)}. \quad (30)$$

Feature $z_1^{\text{bk}}(\cdot; \mu)$ measures the asymmetry of the structure between left and right corners. From symmetry arguments it is easy to verify that

$$z_1^{\text{bk}}(f; \alpha, \beta, E, s_L, s_R) = \frac{1}{z_1^{\text{bk}}(f; \alpha, \beta, E, s_R, s_L)},$$

which implies that by exploiting this feature we should be able to discriminate between the three scenarios $y \in \{1, 4\}$, $y = 2$, $y = 3$.

We then introduce the set of features

$$\mathbf{z}_2^{\text{bk}}(\mu) = [z_2^{\text{bk}}(f^1; \mu), \dots, z_2^{\text{bk}}(f^{Q_1}; \mu)], \quad z_2^{\text{bk}}(f; \mu) = \frac{A_{2,4}^{\text{bk}}(f; \mu) + A_{3,4}^{\text{bk}}(f; \mu)}{A_{1,1}^{\text{bk}}(f; \mu) + A_{4,1}^{\text{bk}}(f; \mu)}. \quad (31)$$

It is easy to verify that the amplitudes $\{A_{i,j}^{\text{bk}}\}_{i,j}$ are monotonically decreasing in α, β (i.e., increases in damping reduce the amplitude of the masses' displacements) and also in s_L, s_R (i.e., increases in the total mass reduce the amplitude). However, while variations in α, β affect all masses, variations in s_L, s_R should be mostly confined to the left and right masses (i.e., masses $(1, j)$ and $(4, j)$ for $j = 1, \dots, 4$). Therefore, the ratio $z_2^{\text{bk}}(\cdot; \mu)$ should reduce the effect of damping on our feature without affecting the effect of s_L, s_R , thereby improving discrimination between $y = 1$ and $y = 4$.

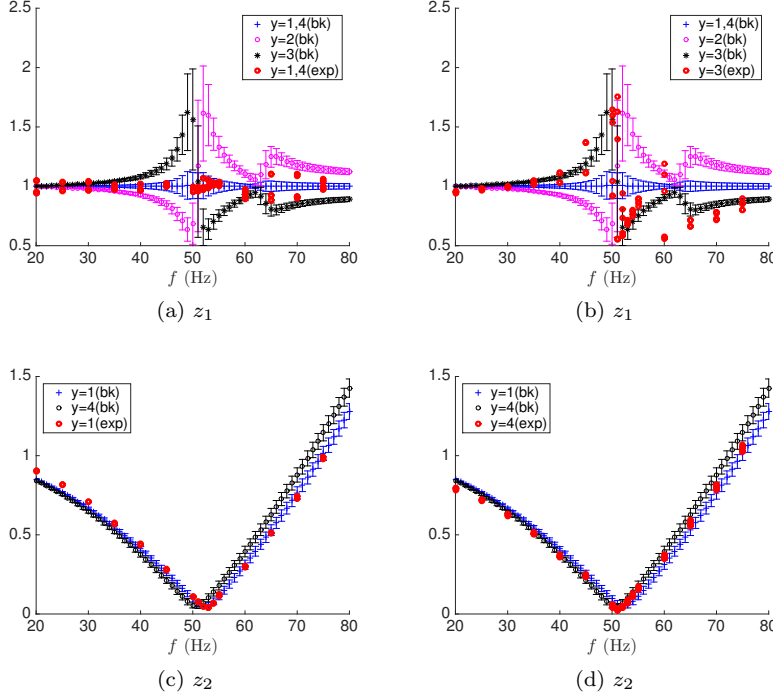


Fig. 5: Microtruss experiment; discrimination capabilities of the features. Figures (a) and (b): behavior of $\{m_q^{1,\text{bk}}(k)\}_q$ and $\{std_q^{1,\text{bk}}(k)\}_q$ for the three classes $k \in \{1, 4\}$, $k = 2$, $k = 3$, and comparison with the experimental data. Figures (c) and (d): behavior of $\{m_q^{2,\text{bk}}(k)\}_q$ and $\{std_q^{2,\text{bk}}(k)\}_q$ for the two classes $k = 1$ and $k = 4$, and comparison with the experimental data. For each experimental configuration, we report results of three independent realizations.

We now demonstrate the effectiveness of our choice of the features for the problem at hand. With this in mind, we introduce a finite-dimensional discretization $\mathcal{P}_{\text{train}}^{\text{bk}}$ of \mathcal{P}^{bk} of cardinality $|\mathcal{P}_{\text{train}}^{\text{bk}}| = n_{\text{train}} = 10^4$. Given the frequencies f^1, \dots, f^{Q_1} , $Q_1 = 16$, we define the in-class mean and standard

deviations:

$$m_q^{\ell, \text{bk}}(k) = \frac{1}{|\mathcal{P}_{\text{train}}^{\text{bk}}(k)|} \sum_{\mu \in \mathcal{P}_{\text{train}}^{\text{bk}}(k)} z_\ell^{\text{bk}}(f^q; \mu), \quad (32a)$$

and

$$\text{std}_q^{\ell, \text{bk}}(k) = \frac{1}{|\mathcal{P}_{\text{train}}^{\text{bk}}(k)| - 1} \sum_{\mu \in \mathcal{P}_{\text{train}}^{\text{bk}}(k)} (z_\ell^{\text{bk}}(f^q; \mu) - m_q^{\ell, \text{bk}}(k))^2, \quad (32b)$$

where $\ell = 1, 2$, and $\mathcal{P}_{\text{train}}^{\text{bk}}(k) = \{\mu \in \mathcal{P}_{\text{train}}^{\text{bk}} : f^{\text{dam}}(\mu) = k\}$. We further consider experimentally the five different nominal system configurations corresponding to (i) $s_L = s_R = 1$, (ii) $s_L = 1, s_R = 2.06$, (iii) $s_L = 1, s_R = 1.53$, (iv) $s_L = s_R = 2.06$, and (v) $s_L = s_R = 1.53$. For each configuration, we perform three independent trials for a total of 15 experimental datapoints. Figures 5 show the behavior of $\{m_q^{\ell, \text{bk}}(k)\}_q$ for $\ell = 1, 2$. For $\ell = 1$, we aggregate the classes $k = 1$ and $k = 4$; for $\ell = 2$, we only consider $k = 1$ and $k = 4$. To take into account the variability of the features due to changes in μ , we report error bars corresponding to twice the in-class standard deviation $\text{std}_q^{\ell, \text{bk}}(k)$. We further report experimental observations from the appropriate class to show the agreement between bk and experimental features.

4.2 Computation of the classifier

Exploiting the reasoning of the previous section, we now introduce the classifier used in the numerical tests: given the set of features $\mathbf{z}_1^{\text{exp}}$ and $\mathbf{z}_2^{\text{exp}}$,

- **Level 1:** distinguish between $\{1, 4\}$, $\{2\}$ and $\{3\}$ based on $\mathbf{z}_1^{\text{exp}}$;
- **Level 2:** if Level 1 returns $\{1, 4\}$, distinguish between $\{1\}$ and $\{4\}$ based on $\mathbf{z}_2^{\text{exp}}$.

We observe that the first layer corresponds to a threeway classification problem, while the second layer corresponds to a binary problem. From a practical perspective, our proposal requires the training of two classifiers: a threeway classifier for the first level and a binary classifier for the second level. We can thus interpret a classifier g as the pair $g = (g_1, g_2)$ where $g_1 : \mathbb{R}^{Q_1} \rightarrow \{0, 2, 3\}$, $g_2 : \mathbb{R}^{Q_1} \rightarrow \{1, 4\}$, and 0 is the label associated to $\{1, 4\}$ for the first level.

In view of the presentation of the numerical results, we define the level-1 and level-2 bk risks:

$$R^{\text{bk}, \text{level } 1}(g) = \int_{\mathcal{P}^{\text{bk}}} \mathcal{L}^{(0,1)}(g_1(\mathbf{z}_1^{\text{bk}}(\mu)), f_1^{\text{dam}}(\mu)) w^{\text{bk}}(\mu) d\mu, \quad (33a)$$

and

$$R^{\text{bk}, \text{level } 2}(g) = \frac{1}{P_1^{\text{bk}} + P_4^{\text{bk}}} \int_{\mathcal{P}^{\text{bk}}(1) \cup \mathcal{P}^{\text{bk}}(4)} \mathcal{L}^{(0,1)}(g_2(\mathbf{z}_2^{\text{bk}}(\mu)), f^{\text{dam}}(\mu)) w^{\text{bk}}(\mu) d\mu,$$

(33b)

where $P_1^{\text{bk}}, \dots, P_4^{\text{bk}}$ are defined in (25), and

$$f_1^{\text{dam}}(\mu) = \begin{cases} 0 & \text{if } f^{\text{dam}}(\mu) \in \{1, 4\}, \\ 2 & \text{if } f^{\text{dam}}(\mu) = 2, \\ 3 & \text{if } f^{\text{dam}}(\mu) = 3. \end{cases} \quad (33c)$$

We observe that $0 \leq R^{\text{bk,level 1}}(g), R^{\text{bk,level 2}}(g) \leq 1$. Similar definitions can be given for level-1 and level-2 experimental risks $R^{\text{exp,level 2}}(g)$ and $R^{\text{exp,level 2}}(g)$.

4.3 Reduced-Basis Approximation

In this section, we discuss how we reduce the computational burden associated with the construction of the dataset $\mathcal{D}_M^{\text{bk}}$ for the microtruss system. More specifically, we wish to speed up computations of the map

$$(f, \mu) \mapsto A_{i,j}^{\text{bk}}(f; \mu)$$

in the limit of many queries using the Reduced Basis (RB) method. With this in mind, we first present the weak formulation of the bk model (section 4.3.1), then we present the RB approximation (section 4.3.2), and finally we provide numerical results to demonstrate the effectiveness of the RB approach (section 4.3.3).

4.3.1 Parametrized microtruss model

We first introduce the weak statement associated with the time-harmonic asymptotic solution to (5) in the configuration-dependent domain Ω_s : given the frequency f , and the bk configuration $\mu = [\alpha, \beta, E, s_L, s_R]$, find $u^{\text{bk}}(f; \mu) \in \mathcal{U}_s := H^1(\Omega_s; \mathbb{C}^2)$ such that

$$\begin{cases} (1 + i\omega_f \beta) E b_{\Omega_s}(u^{\text{bk}}(f; \mu), v) + (-\omega_f^2 + i\omega_f \alpha) \rho L^2 m_{\Omega_s}(u^{\text{bk}}(f; \mu), v) = 0. \\ u^{\text{bk}}(f; \mu)|_{\Gamma^{\text{dir}}} = u^{\text{dir}} \end{cases} \quad (34a)$$

for all $v \in \mathcal{U}_{s,0} = H_{0,\Gamma^{\text{dir}}}^1(\Omega_s; \mathbb{C}^2)$, where $\omega_f = 2\pi f$,

$$m_{\Omega_s}(u, v) = \int_{\Omega_s} u \cdot \bar{v} \, dx, \quad (34b)$$

and

$$b_{\Omega_s}(u, v) = \int_{\Omega_s} \frac{1}{1 + \nu} \text{sym}(\nabla u) : \overline{\text{sym}(\nabla v)} + \frac{1}{(1 + \nu)(1 - 2\nu)} \text{div}(u) \overline{\text{div}(v)} \, dx. \quad (34c)$$

Here, $\bar{\cdot}$ refers to the complex conjugate.

We then introduce a geometric mapping between a parameter-independent domain Ω^{ref} and the configuration-dependent domain Ω_s . With this in mind, we introduce the reference domain $\Omega^{\text{ref}} := \Omega_1^{\text{ref}} \cup \Omega_2^{\text{ref}} \cup \Omega_3^{\text{ref}}$ such that $\Omega_1^{\text{ref}} = \Omega_1$, $\Omega_2^{\text{ref}} = \Omega_2(s_L = 1)$, $\Omega_3^{\text{ref}} = \Omega_3(s_R = 1)$, and we define the affine map

$$\mathcal{T} : \Omega^{\text{ref}} \times [1, 2]^2 \rightarrow \Omega_s, \quad \mathcal{T}(x, s_L, s_R) = \begin{cases} x & \text{if } x \in \Omega_1^{\text{ref}}, \\ x_1 \mathbf{e}_1 + s_L x_2 \mathbf{e}_2 & \text{if } x \in \Omega_2^{\text{ref}}, \\ x_1 \mathbf{e}_1 + s_R x_2 \mathbf{e}_2 & \text{if } x \in \Omega_3^{\text{ref}}, \end{cases} \quad (35)$$

where $\{\mathbf{e}_1, \mathbf{e}_2\}$ is the canonical basis. By tedious but straightforward calculations, we find that, for any $u, v \in H^1(\Omega_s; \mathbb{C}^2)$,

$$(1 + i\omega_f \beta) E b_{\Omega_s}(u, v) + (-\omega_f^2 + i\omega_f \alpha) m_{\Omega_s}(u, v) = \sum_{q=1}^{10} \Theta_q(f; \mu) a^q(\hat{u}, \hat{v}) \quad (36)$$

where $\hat{u}(x) = u(\mathcal{T}(x, s))$, $\hat{v}(x) = v(\mathcal{T}(x, s))$, and the parameter-dependent coefficients $\{\Theta_q\}_{q=1}^{10}$ and the parameter-independent bilinear forms $\{a^q\}_{q=1}^{10}$ are reported in Appendix B. Then, we introduce the lift $u^{\text{lift}} \in H^1(\Omega^{\text{ref}}; \mathbb{C}^2)$ such that $u^{\text{lift}} \equiv 0$ outside Ω_1 , $u^{\text{lift}}(x_{i,j}) = 0$ for all $i, j = 1, \dots, 4$, and $u^{\text{lift}}|_{\Gamma^{\text{dir}}} = u^{\text{dir}}$; we observe that $u^{\text{lift}}(\mathcal{T}^{-1}(x, s_L, s_R))$ does not depend on the values of s_L and s_R .

We can now introduce the parametrized best-knowledge model for the lifted field in the reference configuration and we relate the solution to the experimental measurements. Given a frequency f and bk configuration μ in $\mathcal{P}_f^{\text{bk}}$, we seek the solution $\hat{u}^{\text{bk}}(f; \mu) := u^{\text{bk}}(\mathcal{T}(\cdot, s), f; \mu) - u^{\text{lift}} \in \mathcal{U}_0 = H_{0, \Gamma^{\text{dir}}}^1(\Omega^{\text{ref}}; \mathbb{C}^2)$ to the following variational problem

$$a(\hat{u}^{\text{bk}}(f; \mu), v; f, \mu) = \ell(v; f, \mu), \quad \forall v \in \mathcal{U}_0, \quad (37a)$$

where

$$a(w, v; f, \mu) = \sum_{q=1}^{10} \Theta_q(f, \mu) a^q(w, v), \quad \ell(v; f, \mu) = - \sum_{q=1}^{10} \Theta_q(f, \mu) a^q(u^{\text{lift}}, v), \quad (37b)$$

and

$$(f, \mu) \in \mathcal{P}_f^{\text{bk}} := \mathcal{I}_f \times \mathcal{P}^{\text{bk}}. \quad (37c)$$

Recalling the definition of the map \mathcal{T} (such that $\mathcal{T}^{-1}(x_{i,j}, s_L, s_R) = x_{i,j}$ for all s_L, s_R), and the definition of u^{lift} , we finally find

$$A_{i,j}^{\text{bk}}(f; \mu) = \frac{A_{\text{nom}}}{|\hat{u}_2^{\text{bk}}(x_{2,1}; f, \mu)|} |\hat{u}_2^{\text{bk}}(x_{i,j}; f, \mu)|, \quad (38)$$

where $i, j = 1, \dots, 4$, and $(f, \mu) \in \mathcal{P}_f^{\text{bk}}$. Since $u_2^{\text{bk}}(x_{i,j}; f, \mu) = \hat{u}_2^{\text{bk}}(x_{i,j}; f, \mu) + u^{\text{lift}}(x_{i,j}) = \hat{u}_2^{\text{bk}}(x_{i,j}; f, \mu)$, (37)-(38) is equivalent to (8).

In view of the application of the RB method, we define the norm for \mathcal{U}_0

$$\|u\| := \sqrt{E^{\text{ref}} b_{\Omega^{\text{ref}}}(u, u) + \rho L^2 m_{\Omega^{\text{ref}}}(u, u)}, \quad (39)$$

where $E^{\text{ref}} = 2.8 \cdot 10^9 [\text{Pa}]$, and $m_{\Omega^{\text{ref}}}(\cdot, \cdot)$ and $b_{\Omega^{\text{ref}}}(\cdot, \cdot)$ are defined in (34b) and (34c), respectively. We further define the dual norm of the residual

$$R(u; f, \mu) := \sup_{v \in \mathcal{U}_0} \frac{|a(u, v; f, \mu) - \ell(v; f, \mu)|}{\|v\|}. \quad (40)$$

Finally, we introduce the FE discretization $\mathcal{U}_0^{\mathcal{N}}$ of the space \mathcal{U}_0 based on P4 polynomials and $\mathcal{N} = 14670$ degrees of freedom. We denote by $\hat{u}_{\mathcal{N}}^{\text{bk}}(f; \mu) \in \mathcal{U}_0^{\mathcal{N}}$ the FE approximation of the solution to (37).

4.3.2 Application of the Reduced Basis (RB) method

The key idea of RB is to restrict trial and test spaces in (37) to a low-dimensional space $W_N \subset \mathcal{U}_0^{\mathcal{N}}$ with $N \ll \mathcal{N}$. For a given pair (f, μ) , we define the RB approximation $\hat{u}_{N, \mathcal{N}}^{\text{bk}}(f; \mu) \in W_N$ of $\hat{u}_{\mathcal{N}}^{\text{bk}}(f; \mu)$ as the solution to the N -dimensional variational problem:

$$a(\hat{u}_{N, \mathcal{N}}^{\text{bk}}(f; \mu), v; f, \mu) = \ell(v; f, \mu), \quad \forall v \in W_N. \quad (41a)$$

The RB outputs are then evaluated as

$$\tilde{A}_{i,j}^{\text{bk}}(f; \mu) = \frac{A_{\text{nom}}}{\left| \left(\hat{u}_{N, \mathcal{N}}^{\text{bk}}(x_{2,1}; f, \mu) \right)_2 \right|} \left| \left(\hat{u}_{N, \mathcal{N}}^{\text{bk}}(x_{i,j}; f, \mu) \right)_2 \right|, \quad (41b)$$

$i, j = 1, \dots, 4$, $(f, \mu) \in \mathcal{P}_f^{\text{bk}}$, which yields features (see (30) and (31)):

$$\tilde{\mathbf{z}}_1^{\text{bk}}(\mu) = [\tilde{z}_1^{\text{bk}}(f^1; \mu), \dots, \tilde{z}_1^{\text{bk}}(f^{Q_1}; \mu)], \quad \tilde{z}_1^{\text{bk}}(f; \mu) = \frac{\tilde{A}_{1,4}^{\text{bk}}(f; \mu)}{\tilde{A}_{4,4}^{\text{bk}}(f; \mu)}, \quad (41c)$$

and

$$\tilde{\mathbf{z}}_2^{\text{bk}}(\mu) = [\tilde{z}_2^{\text{bk}}(f^1; \mu), \dots, \tilde{z}_2^{\text{bk}}(f^{Q_1}; \mu)], \quad \tilde{z}_2^{\text{bk}}(f; \mu) = \frac{\tilde{A}_{2,4}^{\text{bk}}(f; \mu) + \tilde{A}_{3,4}^{\text{bk}}(f; \mu)}{\tilde{A}_{1,1}^{\text{bk}}(f; \mu) + \tilde{A}_{4,1}^{\text{bk}}(f; \mu)}. \quad (41d)$$

We generate the space W_N based on snapshots from the bk manifold $\mathcal{M}_{\mathcal{N}}^{\text{bk}} = \{\hat{u}_{\mathcal{N}}^{\text{bk}}(f; \mu) : (f, \mu) \in \mathcal{P}_f^{\text{bk}}\}$. More precisely, we consider a Lagrange ([47]) approximation space W_N as the span of N snapshots $\{\hat{u}_{\mathcal{N}}^{\text{bk}}(f^n; \mu^n)\}_{n=1}^N$, where $\{(f^n, \mu^n)\}_{n=1}^N$ are selected based on the residual-based *weak-Greedy* algorithm (see, e.g., [52, section 7.2.2]): given $\{(f^n, \mu^n)\}_{n=1}^{N-1}$, set (f^N, μ^N) equal to

$$(f^N, \mu^N) := \arg \max_{(f, \mu) \in \mathcal{P}_{f, \text{train}}^{\text{bk}}} \Delta_{N-1}^{\text{bk}}(f, \mu) := R(\hat{u}_{N-1, \mathcal{N}}^{\text{bk}}(f; \mu); f, \mu),$$

where $\mathcal{P}_{f,\text{train}}^{\text{bk}}$ is a suitably finite-dimensional discretization of $\mathcal{P}_f^{\text{bk}}$ of cardinality $|\mathcal{P}_{f,\text{train}}^{\text{bk}}| = n_{\text{train}}$. We recall that this procedure allows us to identify quasi-optimal reduced spaces W_N relative to the Kolmogorov gold standard (see [11] and [18, section 8]).

To reduce the computational cost in the limit of many queries, we pursue an offline/online strategy. During the offline stage (step 2.a in Algorithm 2), we construct the space W_N , and we assemble and store suitable parameter-independent quantities related to the construction of the linear system (41) in terms of the offline expansion (37b). Then, during the online stage (step 2.b in Algorithm 2), we compute the coefficients of the RB solution associated with a suitable basis of W_N , and we evaluate the outputs of interest and subsequently features; the operation count (for a given (f, μ)) depends only on N . The offline stage is performed once and is parameter-independent, while the online stage is repeated for each value of (f, μ) : since the cost of a single online evaluation is significantly less expensive than the corresponding FE evaluation, we can easily amortize the offline computational cost in the limit of many queries.

4.3.3 Numerical results

Figure 6(a) shows the convergence of $\Delta_{N-1}^{\text{bk}}(f^N, \mu^N)$ of the weak-Greedy algorithm ($n_{\text{train}} = 10^3$). We observe that convergence is not monotonic with N : this is to be expected since the problem is not coercive and we consider only Galerkin projection; monotonicity could be guaranteed by appealing to the minimum residual formulation ([41]). We further observe that for $N \gtrsim 15$ the residual stagnates: this is due to round-off errors in residual evaluation; a potential strategy to address this issue is proposed in [15]. Nevertheless, we observe that for $N \gtrsim 15$ we already obtain a sufficient 10^6 reduction in the residual value. Furthermore, Figures 6(b)-(c) show that for $N = 20$ the RB error prediction in feature evaluation is negligible if compared with intra-class differences. In what follows, we may thus effectively equate \hat{u}_N^{bk} and $\hat{u}_{N=20,\mathcal{N}}^{\text{bk}}$.

Finally, we comment on the computational cost. We consider here a P4 FE discretization ($\mathcal{N} = 14670$) and a RB reduced model based on $N = 20$ snapshots. Simulations are performed on a Mac OS-X Intel Core i7 2.8GHz, RAM 16GB. The RB offline cost is roughly $24s$, while the cost of a single input-output evaluation is roughly

$$0.18s \text{ for FE, } 4.4 \cdot 10^{-3}s \text{ for RB.}$$

Assuming that each datapoint $\mathbf{z}^{\text{bk}}(\mu)$ is based on Q_1 frequencies, our RB approach is computationally advantageous if $24s + 4.4 \cdot 10^{-3}s \times MQ_1 < 0.18s \times MQ_1$, or

$$MQ_1 \gtrsim 180.$$

Since we consider $M \approx 10^4$, $Q_1 \approx 10$, the cost of the offline stage is negligible. We also observe that in three space dimensions the RB advantage will further increase.

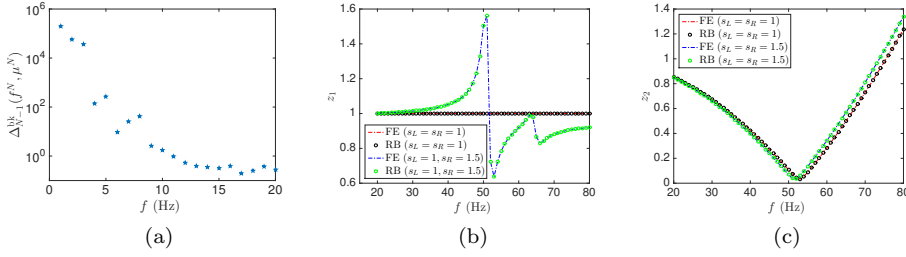


Fig. 6: Microtruss experiment: RB Approximation. Figure (a): convergence of the weak-Greedy. Figures (b) and (c): comparison between FE and RB feature predictions for $\alpha = 5 \cdot 10^{-4}$, $\beta = 10^{-4}$, $E = 2.8 \cdot 10^9$ and three different choices of the geometric parameters.

4.4 Classification results

We consider five distinct classifiers for both levels : one-vs-all Support Vector Machine with Gaussian kernels (ova-SVM,[51, 20, 19]), decision trees ([14]), $\kappa = 5$ -nearest neighbor (kNN, [31, Chapter 13]), artificial neural network with 10 hidden layers (ANN, [12]), and nearest-mean classifier (NMC). We recall that NMC assigns to observations the label of the class of training samples whose centroid $\mathbf{m}(k)$ is closest to observations in a suitable norm. Two standard NMC procedures, which correspond to two different choices of the norm, are

$$g(\mathbf{z}) := \arg \min_{k \in \{1, \dots, K\}} \sum_{q=1}^Q (z_q - m_q^{\text{bk}}(k))^2, \quad (42)$$

and

$$g(\mathbf{z}) := \arg \min_{k \in \{1, \dots, K\}} \sum_{q=1}^Q \frac{(z_q - m_q^{\text{bk}}(k))^2}{std_q^{\text{bk}}(k)}, \quad (43)$$

where $m_q^{\text{bk}}(k)$, $std_q^{\text{bk}}(k)$ are sample mean and sample standard deviations of the training samples of the class k as defined in (32a) and (32b). We standardize data³ for the second level, whereas we do not standardize data for the first level: due to the small variations of z_1 far from resonance, standardization of z_1 increases sensitivity to model error. For NMC, we apply (42) for the first level and (43) for the second level.

We appeal to off-the-shelf Matlab implementations ([43]) of ova-SVM, decision trees, kNN and ANN. More precisely, we rely on `fitcsvm` for binary SVM, `fitctree` for decision trees, `fitknn` for kNN and `train` for ANN. We

³ We recall that standardization of data implies that we train the classifier based on the modified features $\hat{z}_q = \frac{z_q - m_q^{\text{bk}}}{std_q^{\text{bk}}}$ where m_q^{bk} , std_q^{bk} are respectively the sample mean and the sample standard deviation of the training set for all classes.

refer to the Matlab documentation and to the above-mentioned references for further details.

In order to assess performance on experimental data, we consider experimentally the five different nominal system configurations introduced in section 4.1. For each configuration, we consider three independent trials for a total of 15 experimental datapoints. We remark that these experimental datapoints do not include the datapoint employed to estimate \mathcal{P}^{bk} .

We first study performance on synthetic data. More specifically, we study the dependence of the bk risk on the number M of training points. We generate a dataset with $N_{\text{train}} = 10^4$ datapoints corresponding to the following 9 frequencies:

$$\{f^q\}_{q=1}^{Q_1} = \{20.1, 25.1, 30.1, 35.1, 40.1, 65.1, 70.1, 75.1\}.$$

We choose to not consider frequencies close to resonance since the noise is higher. Then, we consider M datapoints for training and $N_{\text{train}} - M$ datapoints for estimating the bk risk. In order to account for the effects of partition, we average results over 100 random splits of the dataset.

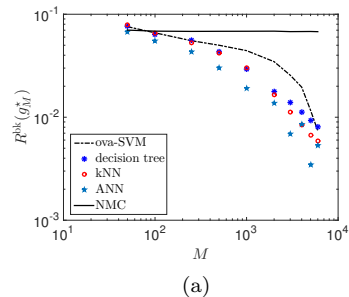


Fig. 7: Microtruss experiment: behavior of the overall (both levels) bk risk $R^{\text{bk}}(g_M^*)$ with M for five different Machine Learning algorithms.

Figure 7 shows the behavior of the bk risk $R^{\text{bk}}(g_M^*)$ with M for the above mentioned classifiers. We observe that performance strongly depends on the amount of training data; this demonstrates empirically the importance of pMOR in the generation of sufficiently large datasets. We further observe that, unlike the other classifiers, performance of NMC does not improve as M increases; this is to be expected since NMC is not in general consistent.

We now study performance for real experimental data. Towards this end, we consider a dataset $\mathcal{D}_{N_{\text{train}}}^{\text{bk}}$ with $N_{\text{train}} = 10^4$ datapoints based on the same 9 frequencies considered for the previous test. We reserve $M = 7 \cdot 10^3$ datapoints for training and validation, and $3 \cdot 10^3$ for testing. As for the previous test, we average results over 100 random splits of the dataset. For this test, we report estimates of the synthetic and experimental risks separately for first and second level (see (33)).

Table 2: Classification performances, $R^{\cdot, \text{level}1}(g)$ and $R^{\cdot, \text{level}2}(g)$, for different learning algorithms for 100 random permutations of learning and test synthetic datasets

Level 1		
	bk-risk $R^{\text{bk}, \text{level}1}(g)$	exp risk (5×3) $R^{\text{exp}, \text{level}1}(g)$
ova-SVM	0.0012	0.0107
decision tree	$7.3 \cdot 10^{-4}$	0.0533
kNN ($k = 5$)	0.0013	0
ANN (10 layers)	$5.9 \cdot 10^{-4}$	0.5773
NMC	0.0161	0
Level 2		
	bk-risk $R^{\text{bk}, \text{level}2}(g)$	exp risk (3×3) $R^{\text{exp}, \text{level}2}(g)$
ova-SVM	0.0096	0.3333
decision tree	0.0013	0.6667
kNN ($k = 5$)	0.0079	0
ANN (10 layers)	0.0017	0.5773
NMC	0.1044	0

Table 2 shows results for both levels and for both synthetic and real data. We observe that kNN and NMC succeed in classifying all the experimental data, while decision trees and Neural Networks perform extremely poorly on experimental data. This demonstrates empirically that SVM, ANN and decision trees are more sensitive to data uncertainty than kNN and NMC. We further observe that, among the choices considered in this work, kNN is the only option that guarantees accurate synthetic and experimental performances.

5 Mathematical analysis

We now discuss the mathematical analysis of our formulation. First, in section 5.1, we propose a probabilistic interpretation of the monitoring problems. This interpretation allows us to address questions related to the well-posedness of the problems stated in section 2.6, and also allows us to discuss the asymptotic properties of the learning machines used for classification. Then, in section 5.2, we propose a general error bound that clarifies the influence of model error on classification performance. Finally, in section 5.3, we discuss in detail a special case that provides insights about the connection between model bias and classification performance.

5.1 Probabilistic interpretation of the monitoring problems

We shall now introduce a probabilistic interpretation of the monitoring problems. This will help us develop and analyze our computational approach. With this in mind, we first recall the definition of $P_{w^{\text{bk}}}$ in (28),

$$P_{w^{\text{bk}}}(A) = \int_{\mathcal{P}^{\text{bk}}} \mathbb{1}_A(\mu') w^{\text{bk}}(\mu') d\mu', \quad A \subset \mathcal{P}^{\text{bk}},$$

and we define the probability measure on $\mathcal{P}^{\text{exp}}, P_{(\mu, \xi)}^{\text{exp}}$, such that

$$P_{(\mu, \xi)}^{\text{exp}}(A \times B) = \int_{\mathcal{P}^{\text{bk}} \times \mathcal{V}} \mathbb{1}_A(\mu) \mathbb{1}_B(\xi) w^{\text{bk}}(\mu') p_{\xi}(\xi') d\mu' d\xi', \quad A \subset \mathcal{P}^{\text{bk}}, \quad B \subset \mathcal{V}. \quad (44)$$

Recalling (18) and (16), it is easy to verify that $P_{w^{\text{bk}}}$ is a probability measure over \mathcal{P}^{bk} , and $P_{(\mu, \xi)}^{\text{exp}}$ is a probability measure over \mathcal{P}^{exp} . As in section 3.1, we denote here by μ a random vector distributed according to $P_{w^{\text{bk}}}$, $\mu \sim P_{w^{\text{bk}}}$; similarly, we denote by (μ, ξ) a random pair distributed according to $P_{(\mu, \xi)}^{\text{exp}}$.

Recalling the definitions of the bk features $\mathbf{z}^{\text{bk}} : \mathcal{P}^{\text{bk}} \rightarrow \mathbb{R}^Q$ and of the damage function $f^{\text{dam}} : \mathcal{P}^{\text{bk}} \rightarrow \{1, \dots, K\}$, we define the random pair

$$(Z^{\text{bk}}, Y) := (\mathbf{z}^{\text{bk}}(\mu), f^{\text{dam}}(\mu)), \quad \mu \sim P_{w^{\text{bk}}}.$$

We further denote by $P_{(Z^{\text{bk}}, Y)}$ the corresponding image probability distribution defined over $\mathbb{R}^Q \times \{1, \dots, K\}$:

$$P_{(Z^{\text{bk}}, Y)}(A \times \{k\}) = \int_{(\mathbf{z}^{\text{bk}}, f^{\text{dam}})^{-1}(A \times \{k\})} w^{\text{bk}}(\mu) d\mu,$$

where $(\mathbf{z}^{\text{bk}}, f^{\text{dam}})^{-1}(A \times \{k\}) := \{\mu \in \mathcal{P}^{\text{bk}} : (\mathbf{z}^{\text{bk}}(\mu), f^{\text{dam}}(\mu)) \in A \times \{k\}\}$ is the pre-image of $A \times \{k\}$. We observe that $P_{(Z^{\text{bk}}, Y)}$ is uniquely identified by the weight w^{bk} , the bk features \mathbf{z}^{bk} and by the damage function f^{dam} . Similarly, we can define the random pair

$$(Z^{\text{exp}}, Y) := (\mathbf{z}^{\text{exp}}(\mu, \xi), f^{\text{dam}}(\mu)), \quad (\mu, \xi) \sim P_{(\mu, \xi)}^{\text{exp}},$$

and the corresponding image probability distribution $P_{(Z^{\text{exp}}, Y)}$.

Recalling the change of variable formula, we can restate the problem statements proposed in section 2.6. In more detail, the monitoring problem (19) can be restated as follows

$$g^{\text{opt}} = \arg \inf_{g \text{ measurable}} R^{\text{exp}}(g) = \mathbb{E}_{(Z^{\text{exp}}, Y) \sim P_{(Z^{\text{exp}}, Y)}} \left[\mathcal{L}^{(0,1)}(g(Z^{\text{exp}}), Y) \right], \quad (45)$$

while the bk monitoring problem can be restated as follows:

$$g^{\text{opt, bk}} = \arg \inf_{g \text{ measurable}} R^{\text{bk}}(g) = \mathbb{E}_{(Z^{\text{bk}}, Y) \sim P_{(Z^{\text{bk}}, Y)}} \left[\mathcal{L}^{(0,1)}(g(Z^{\text{bk}}), Y) \right]. \quad (46)$$

In Appendix A, we rigorously show that if $P_{w^{\text{bk}}}$ is defined on all open sets of \mathcal{P}^{bk} (i.e., $P_{w^{\text{bk}}}$ is Borel-measurable), the features \mathbf{z}^{bk} are continuous with μ and f^{dam} is Borel-measurable, then $P_{(Z^{\text{bk}}, Y)}$ is Borel-measurable. Similarly, if $P_{(\mu, \xi)}^{\text{exp}}$ is Borel-measurable, the features \mathbf{z}^{exp} are continuous with μ and ξ , and

f^{dam} is measurable, then $P_{(Z^{\text{exp}}, Y)}$ is Borel-measurable. This allows us to rigorously study the existence and the uniqueness of solutions to the monitoring problems.

Statements (45) and (46) help us interpret the effect of model error from the perspective of learning. Model error introduces a shift of the statistical properties of the predictors (features). This shows the connection with the notion of *concept drift* ([68, 64]) studied in machine learning, although the latter term commonly refers to changes in the target variable. It is possible to show that this shift can be completely characterized by the probability distribution of $\delta \mathbf{z}$. In this paper, we omit this proof.

We observe that if μ^1, \dots, μ^M are independent identically distributed (iid) samples from $P_{w^{\text{bk}}}$, $\mu \stackrel{iid}{\sim} P_{w^{\text{bk}}}$, then the dataset $\mathcal{D}_M^{\text{bk}}$ consists of M independent samples from the joint distribution $P_{(Z^{\text{bk}}, Y)}$. This has two important implications. First, for a wide class of classifiers (e.g., kernel methods, [63]), we can exploit standard results in learning theory to study the consistency of the classifier g_M^* for the best-knowledge monitoring problem, that is (see, e.g., [65])

$$p \lim_{M \rightarrow \infty} R^{\text{bk}}(g_M^*) = \inf_{g \text{ measurable}} R^{\text{bk}}(g),$$

where $p \lim$ denotes the limit in probability. Second, we can formalize questions related to the Design Of Experiment (DOE) such as frequency selection and sensor placement in a rigorous mathematical fashion, as (grouped-) variable selection problems. In this paper, we do not address the connection between DOE and variable selection, which is the topic of ongoing research.

5.2 Error analysis

We first present two definitions.

Definition 2 Given the classifier $g : \mathbb{R}^Q \rightarrow \{1, \dots, K\}$, we define the k -acceptance region

$$\mathcal{Z}(g, k) := \{\mathbf{z} \in \mathbb{R}^Q : g(\mathbf{z}) = k\}, \quad (47)$$

where $k = 1, \dots, K$.

Definition 3 Given the classifier $g : \mathbb{R}^Q \rightarrow \{0, 1\}$ and the constant $\epsilon > 0$, we define the ϵ -uncertainty indicator E^{bk} as

$$E^{\text{bk}}(g, \epsilon, \mu) := \begin{cases} 0 & \text{if } \mathcal{B}_\epsilon(\mathbf{z}^{\text{bk}}(\mu)) \subset\subset \mathcal{Z}(g, k), \quad \text{for some (unique) } k \in \{1, \dots, K\}; \\ 1 & \text{otherwise;} \end{cases} \quad (48)$$

where $\mathcal{B}_\epsilon(\mathbf{z})$ is the Q -dimensional ball of radius ϵ centered in $\mathbf{z} \in \mathbb{R}^Q$, and $\mathcal{Z}(g, k)$ is defined in (47).

The ϵ -uncertainty indicator E^{bk} is equal to zero if $\mathbf{z}^{\text{bk}}(\mu)$ is sufficiently far from the separating hyper-planes associated with the classifier g . Furthermore, E^{bk} is monotonic increasing in ϵ , and $E^{\text{bk}}(g, \epsilon = 0, \mu) = 0$ unless $\mathbf{z}^{\text{bk}}(\mu)$ lies on a separating hyper-plane. Therefore, it can be interpreted as a measure of local robustness to data uncertainties. We further observe that $E^{\text{bk}}(g, \epsilon, \mu) = 0$ if and only if

$$g(\mathbf{z}^{\text{bk}}(\mu)) = g(\mathbf{z}^{\text{bk}}(\mu) + \delta\mathbf{z}) \quad \forall \delta\mathbf{z} \in \mathcal{B}_\epsilon(\mathbf{0}).$$

Recalling the definition of 0 – 1 loss, we thus find

$$\mathcal{L}^{(0,1)}(g(\mathbf{z}^{\text{bk}}(\mu)), g(\mathbf{z}^{\text{bk}}(\mu) + \delta\mathbf{z})) \leq E^{\text{bk}}(g, \epsilon, \mu) \quad \forall \delta\mathbf{z} \in \mathcal{B}_\epsilon(\mathbf{0}). \quad (49)$$

We formally relate the ϵ -uncertainty indicator (48) to other measures of local robustness that have been proposed in the literature. Given the parameter $\mu \in \mathcal{P}^{\text{bk}}$ and the classifier g , we define

$$r^{\text{bk}}(\mu, g) := \inf_{\mathbf{z} \in \mathcal{Z}^*(g, g(\mathbf{z}^{\text{bk}}(\mu)))} \|\mathbf{z} - \mathbf{z}^{\text{bk}}(\mu)\|_2, \quad (50)$$

where $\mathcal{Z}^*(g, k) = \bigcup_{k' \neq k} \mathcal{Z}(g, k')$ and $\mathcal{Z}(g, k')$ is defined in (47). It is possible to show that we can rewrite the ϵ -uncertainty indicator E^{bk} as

$$E^{\text{bk}}(g, \epsilon, \mu) = \begin{cases} 0 & \text{if } r^{\text{bk}}(\mu, g) > \epsilon; \\ 1 & \text{otherwise.} \end{cases}$$

The quantity $r^{\text{bk}}(\mu, g)$ in (50) is known as *stability radius*, and it is widely used in control theory ([34]), and optimization ([73]) as measure of local robustness. It can be shown (see [61]) that the stability radius is also an instance of Wald's maximin model ([66]), which is employed in statistics and decision theory.

We now present the main result of this section.

Proposition 1 *Let the classifier $g : \mathbb{R}^Q \rightarrow \{1, \dots, K\}$ and the damage function $f^{\text{dam}} : \mathcal{P}^{\text{bk}} \rightarrow \{1, \dots, K\}$ be measurable functions. Let us further define $\epsilon^{\text{bk}} > 0$ as*

$$\epsilon^{\text{bk}} := \|\delta\mathbf{z}\|_{L^\infty(\mathcal{P}^{\text{exp}}; \mathbb{R}^Q)}, \quad \delta\mathbf{z}(\mu, \xi) = \mathbf{z}^{\text{exp}}(\mu, \xi) - \mathbf{z}^{\text{bk}}(\mu). \quad (51)$$

Then, the following hold:

$$R^{\text{exp}}(g) \leq R^{\text{bk}}(g) + \int_{\mathcal{P}^{\text{bk}}} E^{\text{bk}}(g, \epsilon^{\text{bk}}, \mu) w^{\text{bk}}(\mu) d\mu =: R_{\text{UB}}^{\text{exp}}(g, \epsilon^{\text{bk}}), \quad (52)$$

and

$$R^{\text{exp}}(g; k) \leq R^{\text{bk}}(g; k) + \int_{\mathcal{P}^{\text{bk}}(k)} E^{\text{bk}}(g, \epsilon^{\text{bk}}, \mu) w^{\text{bk}}(\mu) d\mu =: R_{\text{UB}}^{\text{exp}}(g, \epsilon^{\text{bk}}, k), \quad (53)$$

for $k = 1, \dots, K$ and for any choice of $p_\xi : \mathcal{V} \rightarrow \mathbb{R}_+$ in (19).

Proof We show only (52), as the proof of (53) is analogous. Applying the triangle inequality, we find

$$\begin{aligned} R^{\text{exp}}(g) &\leq \underbrace{\int_{\mathcal{P}^{\text{exp}}} \mathcal{L}^{(0,1)}(g(\mathbf{z}^{\text{bk}}(\mu)), f^{\text{dam}}(\mu)) w^{\text{bk}}(\mu) p_{\xi}(\xi) d\mu d\xi}_{=(I)} \\ &\quad + \underbrace{\int_{\mathcal{P}^{\text{exp}}} \mathcal{L}^{(0,1)}(g(\mathbf{z}^{\text{bk}}(\mu)), g(\mathbf{z}^{\text{exp}}(\mu, \xi)) w^{\text{bk}}(\mu) p_{\xi}(\xi) d\mu d\xi}_{=(II)} \end{aligned}$$

Then, recalling the definition of w^{bk} in (18), we observe that

$$(I) = \int_{\mathcal{P}^{\text{bk}}} \mathcal{L}^{(0,1)}(g(\mathbf{z}^{\text{bk}}(\mu)), f^{\text{dam}}(\mu)) w^{\text{bk}}(\mu) \underbrace{\int_{\mathcal{Y}} p_{\xi}(\xi) d\xi}_{=1} d\mu = R^{\text{bk}}(g).$$

On the other hand, recalling (49), we find

$$(II) \leq \int_{\mathcal{P}^{\text{bk}}} E^{\text{bk}}(g, \epsilon^{\text{bk}}, \mu) w^{\text{bk}}(\mu) \underbrace{\int_{\mathcal{Y}} p_{\xi}(\xi) d\xi}_{=1} d\mu = \int_{\mathcal{P}^{\text{bk}}} E^{\text{bk}}(g, \epsilon^{\text{bk}}, \mu) w^{\text{bk}}(\mu) d\mu.$$

This follows. \square

Our error analysis clarifies that the online performance of a classifier g depend on two distinct factors: (i) the best-knowledge risk $R^{\text{bk}}(g)$, and (ii) the integral involving the ϵ -uncertainty indicator E^{bk} . The best-knowledge risk $R^{\text{bk}}(g)$ accounts for the nominal performance of the classifier; the integral involving E^{bk} accounts for the robustness of g to data uncertainties and depends on the roughness of the separating hyperplane(s). As observed in section 3, traditional machine learning algorithms aim to minimise the nominal risk (here $R^{\text{bk}}(g)$). If model error is moderate, estimate (52) shows that minimising the nominal risk leads to accurate online performance. On the other hand, if model error is sufficiently large, then this choice does not necessarily lead to accurate decision rules for the online stage.

Before concluding this section, we state a remark.

Remark 2 (The separable case) We discuss the special case in which configuration classes are separable and the classifier g separates them over \mathcal{P}^{bk} , that is

$$R^{\text{bk}}(g) = 0.$$

In this case, provided that the model error is sufficiently small, we can guarantee perfect separation even in presence of model error. Let us define the quantity

$$\delta_k = \inf_{\mu \in \mathcal{P}^{\text{bk}}: g(\mathbf{z}^{\text{bk}}(\mu))=k} \inf_{\mathbf{z} \in \mathcal{Z}^*(g,k)} \|\mathbf{z}^{\text{bk}}(\mu) - \mathbf{z}\|_2.$$

where $\mathcal{Z}^*(g, k) = \bigcup_{k' \neq k} \mathcal{Z}(g, k')$ and $\mathcal{Z}(g, k')$ is defined in (47). Then, if $\epsilon^{\text{bk}} < \min_k \delta_k$, we find that

$$E^{\text{bk}}(g, \epsilon^{\text{bk}}, \mu) \equiv 0, \quad \forall \mu \in \mathcal{P}^{\text{bk}}$$

and exploiting Proposition 1 we find that

$$R^{\text{exp}}(g) = 0;$$

this implies that the classifier g is a solution to problem (19).

5.3 Model bias and experimental risk

We now wish to relate model bias to classification performance for a special case. This will provide insights about the connection between the modelling stage and the inference stage. Let us assume that experimental features can be written as⁴

$$\mathbf{z}^{\text{exp}}(\mu, \xi) = \widehat{\mathcal{F}}(u^{\text{exp}}(\mu, \xi)),$$

where $u^{\text{exp}}(\mu, \xi) \in \mathcal{U}$ is the system state associated with (μ, ξ) , $\mathcal{U} = \mathcal{U}(\Omega)$ is a suitable Hilbert space defined over a domain $\Omega \subset \mathbb{R}^d$, and $\widehat{\mathcal{F}}$ is a linear continuous functional over \mathcal{U} , $\widehat{\mathcal{F}} \in \mathcal{U}'$, with continuity constant C_F . Let us further assume that the best-knowledge features are given by

$$\mathbf{z}^{\text{bk}}(\mu) = \widehat{\mathcal{F}}(u^{\text{bk}}(\mu)),$$

where $u^{\text{bk}}(\mu)$ is the solution to the variational problem

$$G^{\text{bk}}(u^{\text{bk}}(\mu); \mu) = \ell(\mu), \quad \text{in } \mathcal{U}'.$$

Here, we assume that $G^{\text{bk}}(\cdot; \mu)$ is an inf-sup stable linear operator with stability constant $\beta^{\text{bk}}(\mu)$ and $\ell(\mu) \in \mathcal{U}'$ for any $\mu \in \mathcal{P}^{\text{bk}}$.

If we define the *model bias* $f^{\text{bias}} : \mathcal{P}^{\text{exp}} \rightarrow \mathcal{U}'$ as

$$f^{\text{bias}}(\mu, \xi) := G^{\text{bk}}(u^{\text{exp}}(\mu, \xi); \mu) - \ell(\mu), \quad \forall (\mu, \xi) \in \mathcal{P}^{\text{exp}},$$

we obtain

$$\|\delta \mathbf{z}(\mu, \xi)\|_2 = \|\widehat{\mathcal{F}}(u^{\text{exp}}(\mu, \xi) - u^{\text{bk}}(\mu))\|_2 \leq \frac{C_F}{\beta^{\text{bk}}(\mu)} \|f^{\text{bias}}(\mu, \xi)\|_{\mathcal{U}'},$$

which implies that

$$\epsilon^{\text{bk}} = \sup_{(\mu, \xi) \in \mathcal{P}^{\text{exp}}} \|\delta \mathbf{z}(\mu, \xi)\|_2 \leq \sup_{(\mu, \xi) \in \mathcal{P}^{\text{exp}}} \frac{C_F}{\beta^{\text{bk}}(\mu)} \|f^{\text{bias}}(\mu, \xi)\|_{\mathcal{U}'}. \quad (54)$$

Combining estimates (54) with (52), we obtain that the performance of our monitoring system depends on four distinct factors: (i) the nominal performance through the best-knowledge risk $R^{\text{bk}}(g)$, (ii) the robustness of g to

⁴ We consider here the case of static data to not deal with the dependence on frequency.

data uncertainties through the ϵ -uncertainty indicator E^{bk} , (iii) the stability of the PDE through the stability constant $\beta^{\text{bk}}(\mu)$, and (iv) the uncertainty in the model through the bias f^{bias} . We observe that a direct consequence of estimates (52) and (54) is the accommodation of the inevitable, even if small, departure of the physical system from our idealization. However, we observe that (54) is not fully actionable since $\|f^{\text{bias}}(\mu, \xi)\|_{\mathcal{U}'}$ is typically unknown.

6 Conclusions and perspectives

In this paper, we propose a Simulation-Based approach for classification, and we discuss its application to Structural Health Monitoring. We consider a microtruss problem in both a synthetic but also an experimental framework. We exploit recent advances in parametric Model Order Reduction to reduce the computational burden associated with the construction of the offline dataset. Furthermore, we rely on a rigorous mathematical formulation of the classification problem to develop an *a priori* error analysis that links nominal performance on synthetic data to experimental performance. Numerical results show that for certain choices of the classifiers we are able to predict the correct state of damage associated with experimental configurations.

We now identify a number of potential next steps that we wish to pursue in the future.

- *Automatic feature identification*: we wish to exploit the connection between Design Of Experiment (DOE, [28, 49]) and (grouped-) variable selection to automatically identify informative features for classification. By addressing problems of sensor and frequency selection within the context of classification, we can design strategies that are directly informed by the objective function associated to the monitoring problem. We observe that, in the context of regression, similar ideas for sensor placement have been proposed in the experiment design literature (see [39], [13, Section 7.5], [49]).
- *Extension to large-scale structures/high-dimensional configuration spaces*: we wish to consider more realistic engineering situations where definition of damage leads to very high-dimensional configuration spaces. In this respect, we envision that component-based pMOR approaches – and in particular the static-condensation Reduced Basis Element method (scrBE, [37, 23, 60]) – might be naturally suited for this problem due to the local nature of damage generation.
- *Connection with robust optimization*: we wish to explore the connection with Robust Optimization (RO, [10, 9]) to design classification algorithms that are robust to data uncertainty. As discussed in section 5 and empirically shown in section 4.4, robustness to data uncertainties is absolutely crucial to deal with physical problems. We envision that recent advances in RO can help understand and improve the performance of Machine Learning algorithms.
- *Application to other engineering applications*: we wish to apply Simulation-Based Classification to engineering problems other than SHM. More specif-

ically, we wish to consider the application of Simulation-Based Classification to Acoustic Pulse Reflectometry (APR, [1,59]): as SHM, APR can be recast as a classification problem, and the corresponding underlying physical phenomenon is well-described by a parametrized Partial Differential Equation.

Acknowledgements The authors thank Prof. Bernard Haasdonk (University of Stuttgart) for fruitful discussions.

A Existence and uniqueness of the solutions to the monitoring problems

In this appendix, we discuss existence and uniqueness of solutions to the monitoring problems and indeed we develop an explicit — through not readily evaluated — expression for $g^{\text{opt,bk}}$. For the sake of clarity, we recap the definition of $P_{w^{\text{bk}}}$ in (28),

$$P_{w^{\text{bk}}}(A) = \int_{\mathcal{P}^{\text{bk}}} \mathbb{1}_A(\mu') w^{\text{bk}}(\mu') d\mu', \quad A \subset \mathcal{P}^{\text{bk}},$$

and of $P_{(\mu,\xi)}^{\text{exp}}$ in (44),

$$P_{(\mu,\xi)}^{\text{exp}}(A \times B) = \int_{\mathcal{P}^{\text{bk}} \times \mathcal{V}} \mathbb{1}_A(\mu) \mathbb{1}_B(\xi) w^{\text{bk}}(\mu') p_\xi(\xi') d\mu', d\xi'. \quad A \subset \mathcal{P}^{\text{bk}}, \quad B \subset \mathcal{V}.$$

We assume here that $P_{w^{\text{bk}}}$ and $P_{(\mu,\xi)}^{\text{exp}}$ are Borel-measurable, that is they are defined on all open sets of \mathcal{P}^{bk} and \mathcal{P}^{exp} , respectively. A sufficient condition for which $P_{w^{\text{bk}}}$ and $P_{(\mu,\xi)}^{\text{exp}}$ are Borel-measurable is that $w^{\text{bk}} \in L^1(\mathcal{P}^{\text{bk}})$ and $p_\xi \in L^1(\mathcal{V})$. We further recall the random pair

$$(Z^{\text{bk}}, Y) := (\mathbf{z}^{\text{bk}}(\mu), f^{\text{dam}}(\mu)), \quad \mu \sim P_{w^{\text{bk}}},$$

with probability distribution $P_{(Z^{\text{bk}}, Y)}$, and

$$(Z^{\text{exp}}, Y) := (\mathbf{z}^{\text{exp}}(\mu, \xi), f^{\text{dam}}(\mu)), \quad (\mu, \xi) \sim P_{(\mu,\xi)}^{\text{exp}},$$

with probability distribution $P_{(Z^{\text{exp}}, Y)}$.

Next Lemma shows that if \mathbf{z}^{bk} and \mathbf{z}^{exp} are continuous, f^{dam} is Borel-measurable, and $P_{w^{\text{bk}}}$ and $P_{(\mu,\xi)}^{\text{exp}}$ are Borel-measurable, then $P_{(Z^{\text{bk}}, Y)}$ and $P_{(Z^{\text{exp}}, Y)}$ are also Borel-measurable.

Lemma 1 *Suppose that*

1. *the probability measures $P_{w^{\text{bk}}}$ in (28) and $P_{(\mu,\xi)}^{\text{exp}}$ in (44) are Borel-measurable;*
2. *the bk features $\mathbf{z}^{\text{bk}} : \mathcal{P}^{\text{bk}} \rightarrow \mathbb{R}^Q$ and the experimental features $\mathbf{z}^{\text{exp}} : \mathcal{P}^{\text{exp}} \rightarrow \mathbb{R}^Q$ are continuous;*
3. *the discrete function $f^{\text{dam}} : \mathcal{P}^{\text{bk}} \rightarrow \{1, \dots, K\}$ is Borel-measurable.*

Then, the probability measures $P_{(Z^{\text{bk}}, Y)}$ and $P_{(Z^{\text{exp}}, Y)}$ are Borel-measurable on $\mathbb{R}^Q \times \{1, \dots, K\}$.

Proof We only prove that $P_{(Z^{\text{bk}}, Y)}$ is Borel-measurable. The proof of the measurability of $P_{(Z^{\text{exp}}, Y)}$ is analogous. Let $A \subset \mathbb{R}^Q$ be an open set and let $k \in \{1, \dots, K\}$. We must show that $P_{(Z^{\text{bk}}, Y)}(A \times \{k\})$ is well-defined. By construction, we have that

$$P_{(Z^{\text{bk}}, Y)}(A \times \{k\}) = \int_{(Z^{\text{bk}}, Y)^{-1}(A \times \{k\})} w^{\text{bk}}(\mu) d\mu.$$

As a result, we must show that

$$\begin{aligned} (Z^{\text{bk}}, Y)^{-1}(A \times \{k\}) &= \{\mu \in \mathcal{P}^{\text{bk}} : \mathbf{z}^{\text{bk}}(\mu) \in A, f^{\text{dam}}(\mu) = k\} \\ &= (\mathbf{z}^{\text{bk}})^{-1}(A) \cap (f^{\text{dam}})^{-1}(k) \end{aligned}$$

is a Borel set. Since \mathbf{z}^{bk} is continuous and A is open, $(\mathbf{z}^{\text{bk}})^{-1}(A)$ is also open. On the other hand, by assumption, $(f^{\text{dam}})^{-1}(k)$ is Borel. Thesis follows by recalling that the intersection of Borel sets is also Borel. \square

Lemma 1 can be used to prove the following important result related to the existence and uniqueness of solutions to (20) and to (19). We state here only the result for (20). An analogous discussion applies also to the monitoring problem (19).

Proposition 2 *The optimal solution $g^{\text{opt}, \text{bk}}$ to (20) is given by*

$$g^{\text{opt}, \text{bk}}(\mathbf{z}) = \arg \max_{k=1, \dots, K} P_{(Z^{\text{bk}}, Y)}(Y = k | Z^{\text{bk}} = \mathbf{z}). \quad (55)$$

Here, $P_{(Z^{\text{bk}}, Y)}(Y = k | Z^{\text{bk}} = \mathbf{z})$ denotes the conditional probability of the event $\{Y = k\}$ given $\{Z^{\text{bk}} = \mathbf{z}\}$.

Furthermore, if there exists $\epsilon > 0$ such that

$$P_{Z^{\text{bk}}} \left(P_{(Z^{\text{bk}}, Y)}(Y = g^{\text{opt}, \text{bk}}(\mathbf{z}) | Z^{\text{bk}} = \mathbf{z}) \geq \max_{k \neq g^{\text{opt}, \text{bk}}(\mathbf{z})} P_{(Z^{\text{bk}}, Y)}(Y = k | Z^{\text{bk}} = \mathbf{z}) + \epsilon \right) = 1, \quad (56)$$

then any solution g to (20) satisfies $g^{\text{opt}, \text{bk}}(\mathbf{z}) = g(\mathbf{z})$ for $P_{Z^{\text{bk}}}$ -almost every $\mathbf{z} \in \mathbb{R}^Q$.

Proof We first show that (55) is measurable. Recalling [22, Theorem A.24 page 586], since $P_{(Z^{\text{bk}}, Y)}$ is Borel-measurable, if we denote by $P_{Z^{\text{bk}}}$ the corresponding marginal distribution, there exists for $P_{Z^{\text{bk}}}$ -almost every $\mathbf{z} \in \mathbb{R}^Q$ and for $k = 1, \dots, K$ a measurable function $\xi_k^{\text{bk}} : \mathbb{R}^Q \rightarrow \mathbb{R}$ such that $\xi_k^{\text{bk}}(\mathbf{z}) = P_{(Z^{\text{bk}}, Y)}(Y = k | Z^{\text{bk}} = \mathbf{z})$. Recalling that the pointwise maximum of measurable functions is also measurable, this implies that, under the hypotheses of Lemma 1, the function $g^{\text{opt}, \text{bk}}$ in (55) is measurable.

We now observe that

$$\begin{aligned} R^{\text{bk}}(g) &= \int_{\mathbb{R}^Q \times \{1, \dots, K\}} \mathcal{L}^{(0,1)}(g(\mathbf{z}), y) dP_{(Z^{\text{bk}}, Y)}(\mathbf{z}, y) = \int_{\mathbb{R}^Q} \sum_{k \neq g(\mathbf{z})} P_{(Z^{\text{bk}}, Y)}(Y = k | Z^{\text{bk}} = \mathbf{z}) dP_{Z^{\text{bk}}}(\mathbf{z}) \\ &= 1 - \int_{\mathbb{R}^Q} P_{(Z^{\text{bk}}, Y)}(Y = g(\mathbf{z}) | Z^{\text{bk}} = \mathbf{z}) dP_{Z^{\text{bk}}}(\mathbf{z}) \\ &\geq 1 - \int_{\mathbb{R}^Q} \max_k P_{(Z^{\text{bk}}, Y)}(Y = k | Z^{\text{bk}} = \mathbf{z}) dP_{Z^{\text{bk}}}(\mathbf{z}) = R^{\text{bk}}(g^{\text{opt}, \text{bk}}). \end{aligned}$$

Since $g^{\text{opt}, \text{bk}}$ is measurable, this implies that $g^{\text{opt}, \text{bk}}$ is a solution to (20).

Let g be a classifier such that $R^{\text{bk}}(g^{\text{opt}, \text{bk}}) = R^{\text{bk}}(g)$. Using the same reasoning as before, it is possible to verify that

$$R^{\text{bk}}(g) = R^{\text{bk}}(g^{\text{opt}, \text{bk}}) + \int_{\mathbb{R}^Q} \left(P_{(Z^{\text{bk}}, Y)}(Y = g^{\text{opt}, \text{bk}}(\mathbf{z}) | Z^{\text{bk}} = \mathbf{z}) - P_{(Z^{\text{bk}}, Y)}(Y = g(\mathbf{z}) | Z^{\text{bk}} = \mathbf{z}) \right) dP_{Z^{\text{bk}}}(\mathbf{z}).$$

Recalling (56), we find

$$R^{\text{bk}}(g) \geq R^{\text{bk}}(g^{\text{opt}, \text{bk}}) + \epsilon \int_{\mathbb{R}^Q} \mathcal{L}^{(0,1)}(g(\mathbf{z}), g^{\text{opt}, \text{bk}}(\mathbf{z})) dP_{Z^{\text{bk}}}(\mathbf{z}).$$

Then, we must have

$$\int_{\mathbb{R}^Q} \mathcal{L}^{(0,1)}(g(\mathbf{z}), g^{\text{opt}, \text{bk}}(\mathbf{z})) dP_{Z^{\text{bk}}}(\mathbf{z}) = 0,$$

which implies that $g(\mathbf{z}) = g^{\text{opt}, \text{bk}}(\mathbf{z})$ for $P_{Z^{\text{bk}}}$ -almost every $\mathbf{z} \in \mathbb{R}^Q$. \square

B Parametric-affine expansion for the microtruss problem

Below, we report the parameter-dependent coefficients $\{\Theta_q\}_{q=1}^{10}$ and the parameter-independent bilinear forms $\{a^q\}_{q=1}^{10}$ associated with the microtruss problem considered in this work.

$$\Theta_q(f, \mu = [\alpha, \beta, E, s_L, s_R]) = \begin{cases} (1 + i\omega_f \beta)E & q = 1, \\ (-\omega_f^2 + i\omega_f \alpha)\rho L^2 & q = 2, \\ (1 + i\omega_f \beta)s_L E & q = 3, \\ (1 + i\omega_f \beta)E & q = 4, \\ (1 + i\omega_f \beta)s_L^{-1} E & q = 5, \end{cases} \quad \begin{cases} (-\omega_f^2 + i\omega_f \alpha)\rho L^2 s_L & q = 6, \\ (1 + i\omega_f \beta)s_R E & q = 7, \\ (1 + i\omega_f \beta)E & q = 8, \\ (1 + i\omega_f \beta)s_R^{-1} E & q = 9, \\ (-\omega_f^2 + i\omega_f \alpha)\rho L^2 s_R & q = 10, \end{cases} \quad (57a)$$

and

$$a^q(u, v) = \begin{cases} b_{\Omega_1^{ref}}(u, v) & q = 1 \\ m_{\Omega_1^{ref}}(u, v) & q = 2, \\ \int_{\Omega_2^{ref}} \frac{1-\nu}{(1+\nu)(1-2\nu)} \frac{\partial u_1}{\partial x_1} \frac{\partial v_1}{\partial x_1} + \frac{1}{2(1+\nu)} \frac{\partial u_2}{\partial x_1} \frac{\partial v_2}{\partial x_1} dx & q = 3, \\ \int_{\Omega_2^{ref}} \frac{\nu}{(1+\nu)(1-2\nu)} \left(\frac{\partial u_1}{\partial x_1} \frac{\partial v_2}{\partial x_2} + \frac{\partial u_2}{\partial x_2} \frac{\partial v_1}{\partial x_1} \right) + \frac{1}{2(1+\nu)} \left(\frac{\partial u_1}{\partial x_2} \frac{\partial v_2}{\partial x_1} + \frac{\partial u_2}{\partial x_1} \frac{\partial v_1}{\partial x_2} \right) dx & q = 4, \\ \int_{\Omega_2^{ref}} \frac{1-\nu}{(1+\nu)(1-2\nu)} \frac{\partial u_2}{\partial x_2} \frac{\partial v_2}{\partial x_2} + \frac{1}{2(1+\nu)} \frac{\partial u_1}{\partial x_2} \frac{\partial v_1}{\partial x_2} dx & q = 5, \\ m_{\Omega_2^{ref}}(u, v) & q = 6, \\ \int_{\Omega_3^{ref}} \frac{1-\nu}{2(1+\nu)(1-2\nu)} \frac{\partial u_1}{\partial x_1} \frac{\partial v_1}{\partial x_1} + \frac{1}{2(1+\nu)} \frac{\partial u_2}{\partial x_1} \frac{\partial v_2}{\partial x_1} dx & q = 7, \\ \int_{\Omega_3^{ref}} \frac{\nu}{(1+\nu)(1-2\nu)} \left(\frac{\partial u_1}{\partial x_1} \frac{\partial v_2}{\partial x_2} + \frac{\partial u_2}{\partial x_2} \frac{\partial v_1}{\partial x_1} \right) + \frac{1}{2(1+\nu)} \left(\frac{\partial u_1}{\partial x_2} \frac{\partial v_2}{\partial x_1} + \frac{\partial u_2}{\partial x_1} \frac{\partial v_1}{\partial x_2} \right) dx & q = 8, \\ \int_{\Omega_3^{ref}} \frac{1-\nu}{(1+\nu)(1-2\nu)} \frac{\partial u_2}{\partial x_2} \frac{\partial v_2}{\partial x_2} + \frac{1}{2(1+\nu)} \frac{\partial u_1}{\partial x_2} \frac{\partial v_1}{\partial x_2} dx & q = 9, \\ m_{\Omega_3^{ref}}(u, v) & q = 10, \end{cases} \quad (57b)$$

References

1. Amir, N., Barzelay, O., Yefet, A., Pechter, T.: Condenser tube examination using acoustic pulse reflectometry. *Journal of Engineering for Gas Turbines and Power* **132**(1), 014,501 (2010)
2. Au, S.K., Zhang, F.L., Ni, Y.C.: Bayesian operational modal analysis: theory, computation, practice. *Computers & Structures* **126**, 3–14 (2013)
3. Basudhar, A., Missoum, S.: Adaptive explicit decision functions for probabilistic design and optimization using support vector machines. *Computers & Structures* **86**(19), 1904–1917 (2008)
4. Basudhar, A., Missoum, S.: A sampling-based approach for probabilistic design with random fields. *Computer Methods in Applied Mechanics and Engineering* **198**(47), 3647–3655 (2009)
5. Basudhar, A., Missoum, S.: An improved adaptive sampling scheme for the construction of explicit boundaries. *Structural and Multidisciplinary Optimization* **42**(4), 517–529 (2010)

6. Basudhar, A., Missoum, S., Sanchez, A.H.: Limit state function identification using support vector machines for discontinuous responses and disjoint failure domains. *Probabilistic Engineering Mechanics* **23**(1), 1–11 (2008)
7. Ben-Tal, A., El Ghaoui, L., Nemirovski, A.: *Robust optimization*. Princeton University Press (2009)
8. Benedettini, O., Baines, T., Lightfoot, H., Greenough, R.: State-of-the-art in integrated vehicle health management. *Proceedings of the Institution of Mechanical Engineers, Part G: Journal of Aerospace Engineering* **223**(2), 157–170 (2009)
9. Bertsimas, D., Brown, D.B., Caramanis, C.: Theory and applications of robust optimization. *SIAM review* **53**(3), 464–501 (2011)
10. Bertsimas, D., Sim, M.: The price of robustness. *Operations research* **52**(1), 35–53 (2004)
11. Binev, P., Cohen, A., Dahmen, W., DeVore, R., Petrova, G., Wojtaszczyk, P.: Convergence rates for greedy algorithms in reduced basis methods. *SIAM Journal on Mathematical Analysis* **43**(3), 1457–1472 (2011)
12. Bishop, C.M.: *Neural networks for pattern recognition*. Oxford university press (1995)
13. Boyd, S., Vandenberghe, L.: *Convex optimization*. Cambridge university press (2004)
14. Breiman, L., Friedman, J., Stone, C.J., Olshen, R.A.: *Classification and regression trees*. CRC press (1984)
15. Casenave, F., Ern, A., Lelièvre, T.: Accurate and online-efficient evaluation of the a posteriori error bound in the reduced basis method. *ESAIM: Mathematical Modelling and Numerical Analysis* **48**(01), 207–229 (2014)
16. Cawley, P., Adams, R.: The location of defects in structures from measurements of natural frequencies. *The Journal of Strain Analysis for Engineering Design* **14**(2), 49–57 (1979)
17. Chandola, V., Banerjee, A., Kumar, V.: Anomaly detection: A survey. *ACM computing surveys (CSUR)* **41**(3), 15 (2009)
18. Cohen, A., DeVore, R.: Approximation of high-dimensional parametric pdes. *Acta Numerica* **24**, 1–159 (2015)
19. Cortes, C., Vapnik, V.: Support-vector networks. *Machine learning* **20**(3), 273–297 (1995)
20. Cristianini, N., Shawe-Taylor, J.: *An introduction to support vector machines and other kernel-based learning methods*. Cambridge university press (2000)
21. Dawson, B.: Vibration condition monitoring techniques for rotating machinery. *The shock and vibration digest* **8**(12), 3 (1976)
22. Devroye, L., Györfi, L., Lugosi, G.: *A probabilistic theory of pattern recognition*, vol. 31. Springer Science & Business Media (2013)
23. Eftang, J.L., Patera, A.T.: Port reduction in parametrized component static condensation: approximation and a posteriori error estimation. *International Journal for Numerical Methods in Engineering* **96**(5), 269–302 (2013)
24. Fan, W., Qiao, P.: Vibration-based damage identification methods: a review and comparative study. *Structural Health Monitoring* **10**(1), 83–111 (2011)
25. Farrar, C.R., Doebling, S.W., Nix, D.A.: Vibration-based structural damage identification. *Philosophical Transactions of the Royal Society of London A: Mathematical, Physical and Engineering Sciences* **359**(1778), 131–149 (2001)
26. Farrar, C.R., Worden, K.: *Structural health monitoring: a machine learning perspective*. John Wiley & Sons (2012)
27. Fishman, G.: *Monte Carlo: concepts, algorithms, and applications*. Springer Science & Business Media (2013)
28. Franceschini, G., Macchietto, S.: Model-based design of experiments for parameter precision: State of the art. *Chemical Engineering Science* **63**(19), 4846–4872 (2008)
29. Friswell, M., Mottershead, J.E.: *Finite element model updating in structural dynamics*, vol. 38. Springer Science & Business Media (1995)
30. Harris, H.G., Sabnis, G.: *Structural modeling and experimental techniques*. CRC press (1999)
31. Hastie, T., Tibshirani, R., Friedman, J.: *The elements of statistical learning*, vol. 2. Springer (2009)

32. Helton, J.C.: Uncertainty and sensitivity analysis techniques for use in performance assessment for radioactive waste disposal. *Reliability Engineering & System Safety* **42**(2), 327–367 (1993)
33. Hesthaven, J.S., Rozza, G., Stamm, B.: Certified reduced basis methods for parametrized partial differential equations. SpringerBriefs in Mathematics (2015)
34. Hinrichsen, D., Pritchard, A.J.: Stability radii of linear systems. *Systems & Control Letters* **7**(1), 1–10 (1986)
35. Hurtado, J.E.: An examination of methods for approximating implicit limit state functions from the viewpoint of statistical learning theory. *Structural Safety* **26**(3), 271–293 (2004)
36. Hurtado, J.E., Alvarez, D.A.: Classification approach for reliability analysis with stochastic finite-element modeling. *Journal of Structural Engineering* **129**(8), 1141–1149 (2003)
37. Huynh, D.B.P., Knezevic, D.J., Patera, A.T.: A static condensation reduced basis element method: approximation and a posteriori error estimation. *ESAIM: Mathematical Modelling and Numerical Analysis* **47**(01), 213–251 (2013)
38. James, G., Witten, D., Hastie, T., Tibshirani, R.: An introduction to statistical learning. Springer (2013)
39. Joshi, S., Boyd, S.: Sensor selection via convex optimization. *Signal Processing, IEEE Transactions on* **57**(2), 451–462 (2009)
40. Lecerf, M., Allaire, D., Willcox, K.: Methodology for dynamic data-driven online flight capability estimation. *AIAA Journal* **53**(10), 3073–3087 (2015)
41. Maday, Y., Patera, A.T., Rovas, D.V.: A blackbox reduced-basis output bound method for noncoercive linear problems. in *Studies in Mathematics and its Applications*, D. Cioranescu and J. L. Lions, eds., Elsevier Science B. V pp. 533–569 (2001)
42. Mainini, L., Willcox, K.: Surrogate modeling approach to support real-time structural assessment and decision making. *AIAA Journal* **53**(6), 1612–1626 (2015)
43. MATLAB: version 8.5 (R2015a). The MathWorks Inc., Natick, Massachusetts (2015)
44. Mourelatos, Z.P., Kuczera, R., Latcha, M.: An efficient monte carlo reliability analysis using global and local metamodels. In: *Proceedings of 11th AIAA/ISSMO multidisciplinary analysis and optimization conference*, September, Portsmouth, VA (2006)
45. Murphy, K.P.: *Machine learning: a probabilistic perspective*. MIT press (2012)
46. Ortiz, E.M., Clark, G.J., Babbar, A., Vian, J.L., Symos, V.L., Arita, M.M.: Multi source data integration for aircraft health management. In: *Aerospace Conference, 2008 IEEE*, pp. 1–12. IEEE (2008)
47. Porsching, T.: Estimation of the error in the reduced basis method solution of nonlinear equations. *Mathematics of Computation* **45**(172), 487–496 (1985)
48. Prudhomme, S., Oden, J.T.: On goal-oriented error estimation for elliptic problems: application to the control of pointwise errors. *Computer Methods in Applied Mechanics and Engineering* **176**(1), 313–331 (1999)
49. Pukelsheim, F.: *Optimal design of experiments*, vol. 50. siam (1993)
50. Quarteroni, A., Manzoni, A., Negri, F.: *Reduced Basis Methods for Partial Differential Equations: An Introduction*, vol. 92. Springer (2015)
51. Rifkin, R., Klautau, A.: In defense of one-vs-all classification. *The Journal of Machine Learning Research* **5**, 101–141 (2004)
52. Rozza, G., Huynh, D.P., Patera, A.T.: Reduced basis approximation and a posteriori error estimation for affinely parametrized elliptic coercive partial differential equations. *Archives of Computational Methods in Engineering* **15**(3), 229–275 (2008)
53. Rubinstein, R.Y., Kroese, D.P.: *Simulation and the Monte Carlo method*, vol. 707. John Wiley & Sons (2011)
54. Rytter, A.: *Vibration based inspection of civil engineering structures*. Ph.D. thesis, Ph. D. dissertation (1993)
55. Salawu, O.: Detection of structural damage through changes in frequency: a review. *Engineering structures* **19**(9), 718–723 (1997)
56. Sanayei, M., Onipede, O.: Damage assessment of structures using static test data. *AIAA journal* **29**(7), 1174–1179 (1991)
57. Sanayei, M., Saletnik, M.J.: Parameter estimation of structures from static strain measurements. i: Formulation. *Journal of Structural Engineering* **122**(5), 555–562 (1996)

58. Sanayei, M., Saletnik, M.J.: Parameter estimation of structures from static strain measurements. ii: Error sensitivity analysis. *Journal of structural Engineering* **122**(5), 563–572 (1996)
59. Sharp, D., Campbell, D.: Leak detection in pipes using acoustic pulse reflectometry. *Acta Acustica united with Acustica* **83**(3), 560–566 (1997)
60. Smetana, K.: A new certification framework for the port reduced static condensation reduced basis element method. *Computer Methods in Applied Mechanics and Engineering* **283**, 352–383 (2015)
61. Sniedovich, M.: A bird’s view of info-gap decision theory. *The Journal of Risk Finance* **11**(3), 268–283 (2010)
62. Staszewski, W., Boller, C., Tomlinson, G.R.: Health monitoring of aerospace structures: smart sensor technologies and signal processing. John Wiley & Sons (2004)
63. Steinwart, I.: Consistency of support vector machines and other regularized kernel classifiers. *Information Theory, IEEE Transactions on* **51**(1), 128–142 (2005)
64. Tsymbal, A.: The problem of concept drift: definitions and related work. *Computer Science Department, Trinity College Dublin* **106**, 2 (2004)
65. Vapnik, V.N.: *Statistical learning theory*, vol. 1. Wiley New York (1998)
66. Wald, A.: Statistical decision functions which minimize the maximum risk. *Annals of Mathematics* pp. 265–280 (1945)
67. Wenzel, H.: Health monitoring of bridges. John Wiley & Sons (2008)
68. Widmer, G., Kubat, M.: Learning in the presence of concept drift and hidden contexts. *Machine learning* **23**(1), 69–101 (1996)
69. Willis, S.: Olm: A hands-on approach. In: *ICAF 2009, Bridging the Gap between Theory and Operational Practice*, pp. 1199–1214. Springer (2009)
70. Worden, K., Dulieu-Barton, J.: Damage identification in systems and structures. *Int. J. Struct. Health Monit* **3**, 85–98 (2004)
71. Young, W.C., Budynas, R.G.: *Roark’s formulas for stress and strain*, vol. 7. McGraw-Hill New York (2002)
72. Zang, C., Imregun, M.: Structural damage detection using artificial neural networks and measured frf data reduced via principal component projection. *Journal of Sound and Vibration* **242**(5), 813–827 (2001)
73. Zlobec, S.: Characterizing optimality in mathematical programming models. *Acta Applicandae Mathematica* **12**(2), 113–180 (1988)